

AD-A141 669

IONOSPHERIC PHYSICS(U) SACHS/FREEMAN ASSOCIATES INC

1/1

BOWIE MD M SINGH 07 OCT 82 SFA-82-0005

N00173-80-C-0293

UNCLASSIFIED

F/G 4/1

NI

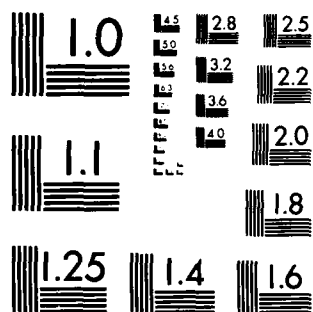
END

DATE

FILED

7-84

DTIC

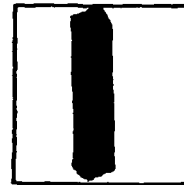


PHOTOGRAPH THIS SHEET

DTIC ACCESSION NUMBER



LEVEL



INVENTORY

Ionospheric Physics, Final

DOCUMENT IDENTIFICATION

Rpt. No. SFA-82-0005

Contract N00173-80-C-0293

7 Oct '82

DISTRIBUTION STATEMENT A

Approved for public release;
Distribution Unlimited

DISTRIBUTION STATEMENT

ACCESSION FOR	
NTIS	GRA&I
DTIC	TAB
UNANNOUNCED	
JUSTIFICATION	
BY	
DISTRIBUTION /	
AVAILABILITY CODES	
DIST	AVAIL AND/OR SPECIAL
<i>A/1</i>	

DISTRIBUTION STAMP

DTIC
ELECTE
S **D**
MAY 21 1984
D

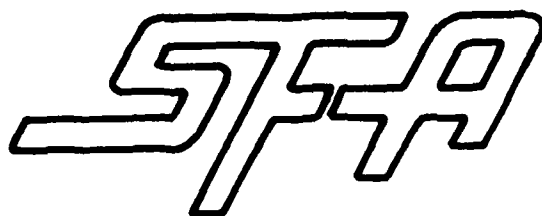
DATE ACCESSIONED



84 05 17 059

DATE RECEIVED IN DTIC

PHOTOGRAPH THIS SHEET AND RETURN TO DTIC-DDA-2



AD-A141 669

FINAL REPORT


IONOSPHERIC PHYSICS

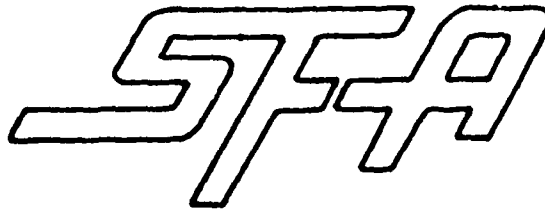
M. Singh, PhD
Sachs/Freeman Associates, Inc.
14300 Gallant Fox Lane
Suite 214
Bowie, MD 20715

07 October 1982

SACHS/FREEMAN ASSOCIATES, INC.

14300 GALLANT FOX LANE, SUITE 214, BOWIE, MARYLAND 20715 301-262-4400





FINAL REPORT

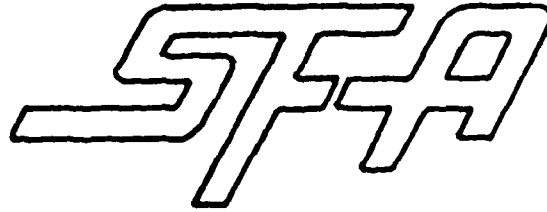
IONOSPHERIC PHYSICS

M. Singh, PhD
Sachs/Freeman Associates, Inc.
14300 Gallant Fox Lane
Suite 214
Bowie, MD 20715

07 October 1982

SACHS/FREEMAN ASSOCIATES, INC.

14300 GALLANT FOX LANE, SUITE 214, BOWIE, MARYLAND 20715 301-262-4400



Security Classification: Unclassified

SFA82-0005

IONOSPHERIC PHYSICS

M. Singh, PhD
Sachs/Freeman Associates, Inc.
14300 Gallant Fox Lane
Suite 214
Bowie, MD 20715

07 October 1982

Final Report for Period 31 July 1980 ~ 31 August 1982

Distribution Statement:
NRL Code 4187, 1230

Prepared for:

NAVAL RESEARCH LABORATORY
Space Sciences Division, Code 4187
4555 Overlook Avenue, SW
Washington, DC 20375

SACHS/FREEMAN ASSOCIATES, INC.

14300 GALLANT FOX LANE, SUITE 214, BOWIE, MARYLAND 20715 301-262-4400

SECURITY CLASSIFICATION OF THIS PAGE (When Data Entered)

REPORT DOCUMENTATION PAGE		READ INSTRUCTIONS BEFORE COMPLETING FORM
1. REPORT NUMBER SFA-RD-80-C-0293	2. GOVT ACCESSION NO.	3. RECIPIENT'S CATALOG NUMBER
4. TITLE (and Subtitle) IONOSPHERIC RESEARCH		5. TYPE OF REPORT & PERIOD COVERED 31 July 1980 - 31 Aug 1982 Final Report
		6. PERFORMING ORG. REPORT NUMBER SFA-82-0005
7. AUTHOR(s) M. Singh, PhD		8. CONTRACT OR GRANT NUMBER(s) N00173-80-C-0293
9. PERFORMING ORGANIZATION NAME AND ADDRESS Sachs/Freeman Associates, Inc. 14300 Gallant Fox Lane, Suite 214 Bowie, Maryland 20715		10. PROGRAM ELEMENT, PROJECT, TASK AREA & WORK UNIT NUMBERS
11. CONTROLLING OFFICE NAME AND ADDRESS Naval Research Laboratory Space Sciences Div., Code 4187 4555 Overlook Ave., SW, Washington, DC 20375		12. REPORT DATE October 7, 1982
		13. NUMBER OF PAGES
14. MONITORING AGENCY NAME & ADDRESS (if different from Controlling Office) DCASMA, Baltimore Room 200, 300 E. Joppa Road Towson, MD 21204		15. SECURITY CLASS. (of this report) Unclassified
		15a. DECLASSIFICATION/DOWNGRADING SCHEDULE
16. DISTRIBUTION STATEMENT (of this Report) Approved for public release; distribution unlimited.		
17. DISTRIBUTION STATEMENT (of the abstract entered in Block 20, if different from Report)		
18. SUPPLEMENTARY NOTES		
19. KEY WORDS (Continue on reverse side if necessary and identify by block number) F-Region irregularities; ionospheric; S3-4 Satellite		
20. ABSTRACT (Continue on reverse side if necessary and identify by block number) The Ionospheric Diagnostic Section of the Upper Air Physics Branch, Space Sciences Division requires understanding similarities and differences between polar and equatorial spread-F irregularities. This report discusses equatorial investigations with major technical, scientific and engineering advances contributing to the current understanding and future plans for adaptive communications system design and ionospheric modification and control. In this report, the S3-4 satellite data analyses is summarized.		

1.1 INTRODUCTION

The Upper Air Physics Branch (Code 4120) at the Naval Research Laboratory (NRL) conducts upper air and astrophysical research by means of rockets and satellites. This research includes studies of the wavelength distribution of solar radiation and the time variations of such emissions as well as the resonant scattering of solar radiation by atmospheric species. The Branch also conducts a rocket astronomy program to study nighttime ultraviolet and x-ray radiations from galactic sources and studies the effects of radiation and particles incident on the Earth's atmosphere. This data is used to determine the ionic and molecular composition, temperature and density of the high atmosphere. The Ionospheric Diagnostic Section is involved with measurement of ionospheric plasma phenomena; specifically, F-region irregularities at equatorial and high latitudes.

Accumulating information regarding the equatorial F-region ionosphere has proven to be important for the communications and ionospheric sciences. This interest has brought considerable intensity into equatorial investigations with major technical, scientific, and engineering advances contributing to the current understanding and future plans for adaptive communications system design and ionospheric modification and control. In this report the S3-4 satellite data analysis is summarized.

2.1 EQUATORIAL IONOSPHERIC IRREGULARITIES

The cause-effect relationship for the equatorial ionospheric irregularities was investigated by analyzing the S3-4 and Plumex-1 data. The results of S3-4 satellite data analyses can be summarized as follows:

- ° Near the nighttime equator there are irregularity structures with depletions in plasma density up to 3 orders of magnitude and range in horizontal extent from ten's of kms to less than 1 km. These depletions show east-west asymmetry with more spectral strength on the western wall of the depletions, suggesting more scintillations on the western wall. The mean ion mass, as inferred from the ratio square $(I_e/I_i)^2$, is more inside the depletions in most of the depletions suggesting more molecular ions inside the depletions.

- ° The power spectral analyses of S3-4 data inside the irregular structures show that in the intermediate wavelength domain (2km - 25m), the power spectral index is $2.4(\pm 0.4)$. This supports the belief that these irregularities are produced by collisional Rayleigh-Taylor instability. Simultaneous power spectral analyses on electron density and mean-ion-mass have shown a general behavior tending to lower power and soften spectra in ion mass fluctuations as compared with the fluctuations in total plasma density.

- ° The ionospheric irregularities during the equatorial spread-F conditions are known to range from ten's (may be hundreds) of kms to 1 meter or even 11 cm. To investigate the plasma process(es) responsible for the generation of these irregularities which range six orders of magnitude in the wavelength domain, the histograms of spectral indices (obtained by FFT analyses of a number of S3-4 orbits) in the different wavelength domains have been drawn. The long wavelength domain ($50 \text{ km} > \lambda > 1 \text{ km}$) lies near 1.5 while for intermediate

($1\text{km} > \lambda > 20\text{m}$) and transitional ($100\text{m} > \lambda > 10\text{m}$) wavelengths ($\lambda > 10\text{m}$) two types of phenomena have been observed on the power spectra: the peaks at frequencies of few hundreds Hz corresponding to wavelengths of few meters and a break in FFT near 3 meter wavelength. These are explained on the basis of excitation of drift wave and lower-hybrid instability respectively.

The total spectra ranging from ten's of kms to few meters is explained by the concept of cascading of irregularities or heirachy of instabilities. The equatorial spread-F starts at wavelengths range of hundreds of kms to tens of kms by either TID s or gravity waves. The longer wavelengths generate the conditions which are ripe for the onset of Rayleigh-Taylor (R-T) instability. The gradient scale sizes for R-T instability is near 20 km. Once R-T instability has taken over, it produces the gradient scale sizes of few hundred meters which start gradient driven drift instability in the transitional wavelength domain. This phenomena of cascading of irregularities to shorter and shorter sizes produces conditions for excitation of drift waves, parametric instabilities and lower-hybrid instabilities.

The most significant results of the investigations have been the two-dimensional picture of depletions and the understanding of different plasma processes in the different wavelength domains of ionospheric equatorial irregularities.

3.1 LONGITUDINAL VARIATIONS IN EQUATORIAL IRREGULARITIES

One of the advantages of STP/S3-4 was that it was sun-synchronous and polar orbit satellite which made it possible to study the longitudinal variations in equatorial irregularities, as well as global coverage. During the six month (March-September 1978) life of the satellite, about 24 percent orbits of the total number of orbits which covered the nighttime equator observed the ionospheric irregularities. Although the irregularities can be present at almost any longitude, 50 percent of the observed irregularities lie in the narrow longitude zones of $0-15^\circ$ and $165-195^\circ\text{E}$.

4.1 CALCULATION DEVELOPMENT

To perform the above tasks, a large number of routines were developed for both PDP 11/10 and PDP 11/34 minicomputers. A partial list of these routines is given below:

- ° To read the data from tapes provided by Aerojet for S3-4 data.
- ° Calculation and the plot routines for the saturation currents ($I_B(E)$, $I_B(I)$) and the ratio square $[(I_B(E)/I_B(I))^2]$ for S3-4, Plumex-1, and DNA/PLACES data in various formats.
- ° Plot routines for I-V characteristics for S3-4 data and the temperature calculation routine.
- ° Calculation of gradient scale length both for S3-4 and Plumex-1 data and subsequent plot routines.
- ° FFT analyses routine along with the addition of window and filter.
- ° Calculation and plot routine for a chapman layer used in BIME simulations and SAR applications.

5.1 SCIENTIFIC DOCUMENTATION

Presentations:

1. "High resolution satellite measurements of equatorial F-region irregularities", presented at AGU Spring meeting in Toronto, Ontario (May, 1980).
2. "Satellite and rocket observations of equatorial spread-F irregularities", presented at 6th ISEA meeting in Aguadilla, Puerto Rico (July, 1980).
3. "The STP/S3-4 satellite expt; equatorial F-region irregularities", presented at I.E.S., Alexandria, VA (April, 1981).
4. "Spectral classification of equatorial irregularities", presented at AGU spring meeting in Baltimore, MD (May, 1981).
5. "The STP/S3-4 satellite experiment: Equatorial F-region irregularities", presented at U.R.S.I. meeting, Washington, DC (August, 1981).
6. "Synoptic measurements of small-scale variations in the midlatitude ionosphere with a radio astronomy interferometer", presented at AGU fall meeting, San Francisco, CA (Dec., 1981).
7. "Drift waves in equatorial spread-F", presented at AGU spring meeting, Philadelphia, PA (May, 1982).
8. "Expanded probe diagnostics in multi-component plasmas", presented at AGU spring meeting, Philadelphia, PA (May, 1982).

Publications:

1. "Satellite and rocket observations of equatorial spread-F Irregularities", J. Atmos. Terr. Phys. 43, 779 (1981).
2. "The STP/S3-4 Satellite Experiment: Equatorial F-region Irregularities", NRL Memo Rept. 4531, proc. I.E.S., 228, 1982.

3. "The STP/3-4 Satellite Experiment: High Latitude Large Scale Density Irregularities", NRL Memo Rept. 4514, proc. I.E.S., 431, 1982.
4. "The S3-4 Ionospheric Irregularities Satellite Experiment: Probe detection of multi-ion component plasmas and associated effects on instability processes", NRL Memo Rept. 4728. Also in Astrophys. and Space Science (1982).
5. "An Atlas of Ionospheric F-region structures as Determined by the NRL-747/S3-4 Ionospheric Irregularities Satellite Investigations", NRL Memo Rept. 4862, 1982.
6. "The Two-dimensional Wave Number Spectrum Classification of the Equatorial Spread-F", J. Geophys. Res. (to be submitted).

Satellite and rocket observations of equatorial spread-*F* irregularities: a two-dimensional model

E. P. SZUSZCZEWICZ, M. SINGH* and J. C. HOLMES

E. O. Hulburt Center for Space Research, Naval Research Laboratory, Washington, DC 20375, U.S.A.

Abstract—Recent rocket and satellite measurements of equatorial *F*-region irregularities have been able to resolve wavelengths comparable to the meter-size sensitivities of the Jicamarca and Altair radar backscatter techniques. In a July 1979 rocket campaign at the Kwajalein Atoll, vertical profile measurements by 'in situ' plasma probes showed the *F*-region marked by a number of large scale plasma depletions, each having its own distribution of smaller scale irregularities and a trend toward a co-location of the more intense irregularities with positive gradients of larger scale features. Similar measurements on the S3-4 Ionospheric Irregularities Satellite have shown large scale depletions (1–3 orders of magnitude) with east–west asymmetries that point toward the western wall as the sight for the more intense plasma density fluctuations. The combined rocket and satellite measurements provide a two-dimensional model of macroscopic *F*-region depletions with small structures tending to develop more readily on the top and western boundaries. The model and associated power spectral analyses is in concert with a developing catalog of radar observations and the predictions of numerical simulations which employ the Rayleigh–Taylor instability as the primary mechanism for the generation of intermediate wavelength irregularities.

1. INTRODUCTION

Recently, there have been considerable advances in the understanding of equatorial spread-*F* as a result of improved ground based radar observations and coordinated *in situ* measurements. The long standing Jicamarca radar results [e.g. WOODMAN and LAHOZ (1976) and associated references] have been studied in greater detail by the expanded capabilities of the Altair radar facility in the Kwajalein Atoll (TSUNODA and TOWLE, 1980). These more recent results have investigated plume development in an east–west cross-section and provided some tentative identification of plume elements with local *F*-region plasma depletions (TSUNODA, 1980a, b).

Early efforts to examine the exact relationship between radar plumes and ionospheric depletions by performing simultaneous *in situ* and ground-based radar observations (KELLEY *et al.*, 1976; MORSE *et al.*, 1977) were limited to conditions of bottomside spread-*F* and required extrapolations in space and time to establish correlations. These frustrations, as well as two unsuccessful attempts at Kwajalein in 1977 and 1978, were finally relieved by the successful DNA/PLUMEX campaign in 1979 (SZUSZCZEWICZ *et al.*, 1980a) which definitively established the co-location of intense radar

returns with the upper region of a topside *F*-layer depletion. The PLUMEX results also provided the first vertical profile of large-scale plasma depletions with superimposed distributions of smaller scale irregularities.

In an attempt to establish a 2-dimensional east–west *in situ* profile that complements the developing catalog of Altair observations, we present in this paper a composite of rocket and satellite observations, from the PLUMEX campaign on the one hand and the S3-4 satellite on the other. These results are summarized in subsequent sections and synthesized in a way that suggests a two-dimensional model of macroscopic *F*-region depletions with smaller scale structures tending to develop more readily on the top and western boundaries.

2. ROCKET-BORNE MEASUREMENTS

The coordinated measurements of equatorial spread-*F* conducted during July 1979 at the Kwajalein Atoll involved the launch of two instrumented rocket payloads designed to probe the detailed *in situ* structure of the turbulent ionospheric plasma. The first launch operation (PLUMEX I; 17 July 1979; 0031:3025 LT) was conducted during the late phase in the development and decay of spread-*F*. The associated results and discussions of ground-based and rocket-borne diagnostics have been presented by SZUSZCZEWICZ *et al.* (1980a, b).

*Sachs/Freeman Associates, Inc., Bowie, MD 20715.
On leave from Punjabi University, Patiala, India.

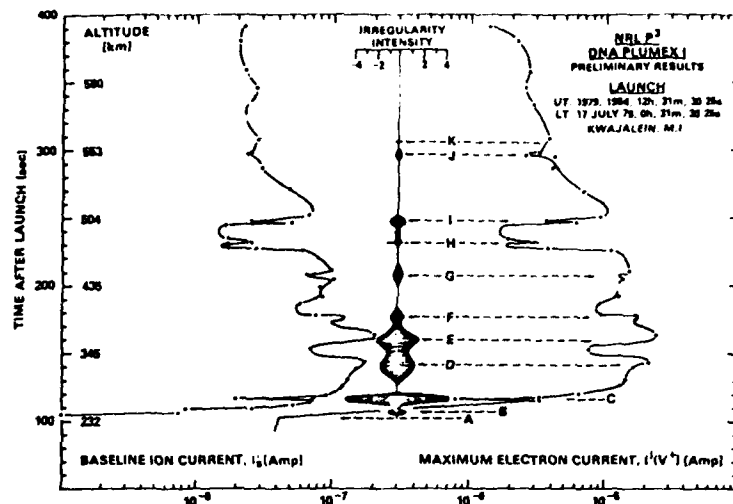


Fig. 1. Relative electron density profile of macroscale features as measured simultaneously by ion and electron saturation probe currents collected on the upleg trajectory of PLUMEX I. 'Irregularity intensity' provides an approximate measure of smaller scale structure with a ± 4 irregularity approximately equal to $\pm 80\%$ fluctuations about a linear detrend. (From SZUSZCZEWICZ et al., 1980.)

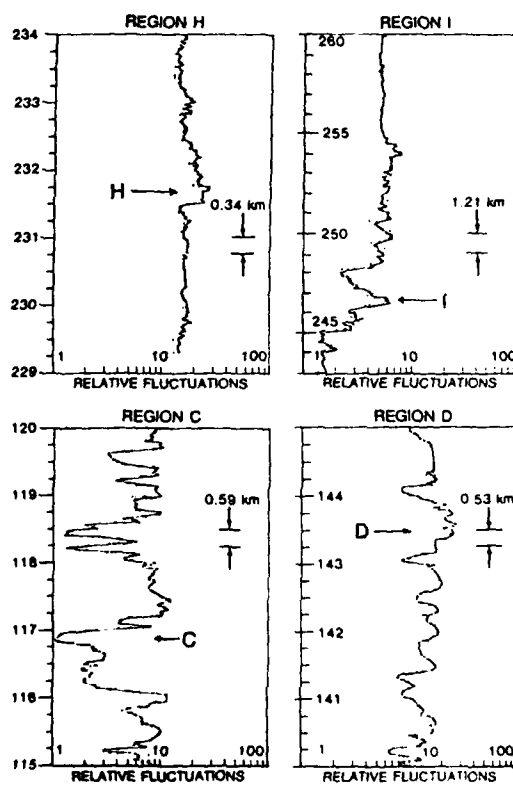


Fig. 2. Expanded views of density fluctuations observed in regions C, D, H and I of Fig. 1.

For purposes of comparison with subsequent presentations of S3-4 satellite data we show here in Fig. 1 the upleg measurements of relative density as presented by correlated ion- (I_B') and electron-saturation $I_e'(V')$ currents collected by a pair of on-board pulsed-plasma-probes (HOLMES and SZUSZCZEWICZ, 1975; SZUSZCZEWICZ and HOLMES, 1980) in the PLUMEX I operation. The ordinate has a linear scale for time-after-launch with altitude superimposed at 50 s increments. (Because ion and electron saturation currents have significantly different sensitivities to velocity, sheath and magnetic field effects, variations in I_B' and $I_e'(V')$ not mutually corroborated were attributed to the various aspect sensitivities and excluded from Fig. 1. This approach facilitated analysis, reduced computer time, and established credibility in the interpretation of the curves as relative electron density profiles.)

The results in Fig. 1 show that a number of major depletions ($\Delta N_e/N_e \leq 0.9$) were distributed throughout the F-region. Each of the large scale depletions (identified alphabetically) has its own distribution of irregularities, illustrated in Fig. 2 by the expanded view of regions C, D, H and I. It is clear that C is not a single narrow biteout but a collection of rather large irregular structures extending over a total altitude domain of about 12 km. (Vehicle velocity in region C was 2.4 km/s.) To develop a quantitative view of irregularity fluctuations observed in the F-region, contiguous linear detrends over 4-s intervals were executed throughout the entire upleg trajectory. The variations about those linear detrends were then plotted in Fig. 1 as 'Irregularity Intensity,' with a maximum relative scale of ± 4 . A fluctuation as great as ± 4 approximately represents a $\pm 80\%$ fluctuation about the linear detrend. (Correlation of these results with macroscale gradients and Altair backscatter contours are discussed by SZUSZCZEWICZ *et al.*, 1980a). The results show that the most intense irregularities occurred on the bottomside gradient (region C) with corresponding measurements at all other altitudes at a much lower level. We note that the fluctuations in the largest depletion (region H-I) are smaller than those at C. Furthermore, the fluctuations at C, D, E and I are more intense than at adjacent locations; and C, D, E and I are collocated with positive density gradients of large scale features.

3. S3-4 SATELLITE RESULTS

While rocket-borne instrumentation can provide vertical profiles of irregularities, a circular or near-circular orbiting satellite with high resolution in-

strumentation is required to assemble irregularity intensities and power law behavior in the horizontal plane. The S3-4 satellite carries just such an experiment.

The S3-4 ionospheric irregularities experiment employs a pair of pulsed-plasma-probes (HOLMES and SZUSZCZEWICZ, 1975; SZUSZCZEWICZ and HOLMES, 1980) on a polar (96.4° inclination), sun-synchronous (2230 h LT, equatorial crossing), F-region orbiting satellite. The experiment provides direct measurements of the ionospheric state (N_e , T_e), its condition of irregularity (δN_e), and associated electron density fluctuation power spectra $[P(k)]$ with 5–20 m resolution.

Figure 3 presents a sample of relative electron density data collected during a nighttime equatorial crossing with the satellite orbiting at an altitude of 240 km with a velocity of 7.53 km/s. The velocity component perpendicular to the geomagnetic field is 2.0 km/s. 50 s of data are displayed covering a total horizontal extent equal to 366 km, moving from east-to-west with increasing time.

While the data represents a transit from the southeast to the northwest, our discussions and associated interpretations will assume that all variations along the magnetic field are negligible. We therefore interpret our results in the framework of a two-dimensional system, perpendicular to the magnetic field. This assumption is similarly employed in theoretical analyses of equatorial spread-F (e.g. SCANNAPIECO and OSSAKOW 1976) and supported by 6300 Å airglow intensity measurements of F-region depletions which show significantly greater variation in east-west extent than north-south (WEBER *et al.*, 1978). Our discussions will also assume temporal variations to be nonexistent during the satellite traversal across any given depletion (typically 10 s or less in Fig. 3). We consider this a reasonable position since saturation times for unstable Rayleigh-Taylor modes are of the order of 4000 s (KESKINEN *et al.*, 1980a) and F-layer vertical drift velocities are generally in the 10–20 m/s range (e.g. SZUSZCZEWICZ *et al.*, 1980). In neither case should our interpretations be influenced by a 10 s time lapse as the satellite passes from the eastern to the western boundary of a depletion.

The data reveal four large scale depletions ranging up to 98 km wide and a factor of 300 in depth, with smaller scale structure visible down to a fraction of a kilometer. The upper portion of Fig. 3 presents 'irregularity intensity' as measured by relative fluctuations about continuous 0.27 s (2.1 km) linear detrends.

Further discussion is facilitated by identifying

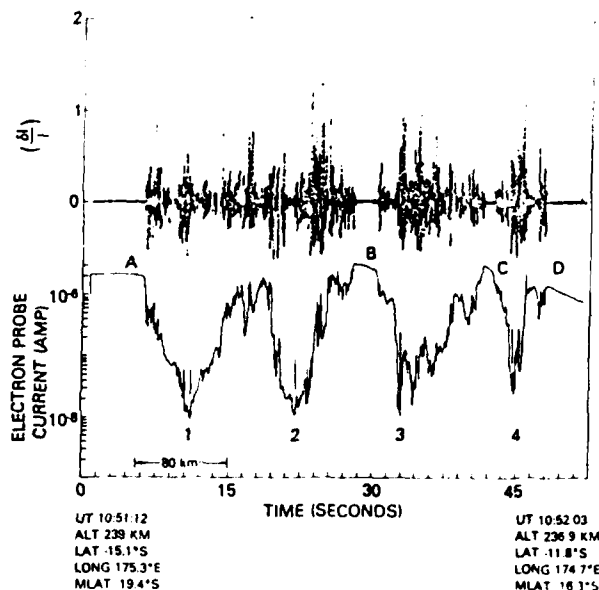


Fig. 3. The electron density variations as measured by the electron probe aboard S3-4 on rev. No. 2123. On the top is the irregularity intensity ($\delta I/I$) determined over contiguous 2.1 km intervals throughout the depletions.

certain features in Fig. 3. First, there are clearly defined regions of undisturbed background ionosphere, marked alphabetically A through D; the smoothness of the relative density and the corresponding 0% fluctuations attest to their undisturbed nature. The eastern boundary is defined as the region of density gradient moving westward from an undisturbed domain to the least lower bound of relative plasma density in the depletion. Everything to the west of that minimum is defined as the western boundary. Admittedly these definitions leave no room for a region that might be called the 'depletion center,' but depletions 3 and 4 suggest that there is no easily defined 'depletion center.' This is also borne out by other sets of P_1 data.

Focussing on depletions 3 and 4, we see that the irregularity intensities are 2 to 3 times larger on the western boundary than on its eastern counterpart. This same relationship is true in depletions 1 and 2, but only after a qualification that suggests that 1 and 2 are halves of a larger depletion bounded by A and B. This is supported in part by the nonexistence of a quiescent ionosphere between the two. When viewed from this perspective the western boundary is approximately twice as intense in irregularity intensity as the eastern boundary.

Signatures in irregularity strengths and relationships to plasma instability mechanisms can be

further explored through power spectral density analyses. We present in Fig. 4 just such results for each of the boundaries in Fig. 3 (1E and 1W refer respectively to the eastern and western boundary of depletion number 1). Power spectral analyses are presented across the boundaries of each of the four depletions with spectral indices (η , in a spectral fit to $P = P_0 f^{-\eta}$) ranging from 1.9 to 2.3. (These indices are in agreement with the work of KESKINEN *et al.* (1980) where numerical simulations predict $\eta = 2.0$ to 2.5 for horizontal irregularity structures perpendicular to \vec{B} . This result runs parallel to an earlier comparison (SZUSZCZEWICZ and HOLMES, 1980; KESKINEN *et al.* 1980b) which showed that the power spectral index across region C in PLUMEX I also agreed with the predictions of KESKINEN *et al.* (1980a) in the vertical plane.) More important to the discussion of east-west asymmetries is the ratio of the spectral strengths (P_0) across the two boundaries. By defining P_1 as the $P_0(\text{West})/P_0(\text{East})$, we find the ratio P_1 to extend from 1.4 to 11.3, i.e. the irregularity spectral strength on the western wall is 1.4 to 11.3 times more intense than on the eastern counterpart.

These results are in concert with the radar observations of TSUNODA (1979) which show that the bottomside backscatter strength is often asymmetric in the east-west plane, with the western side of

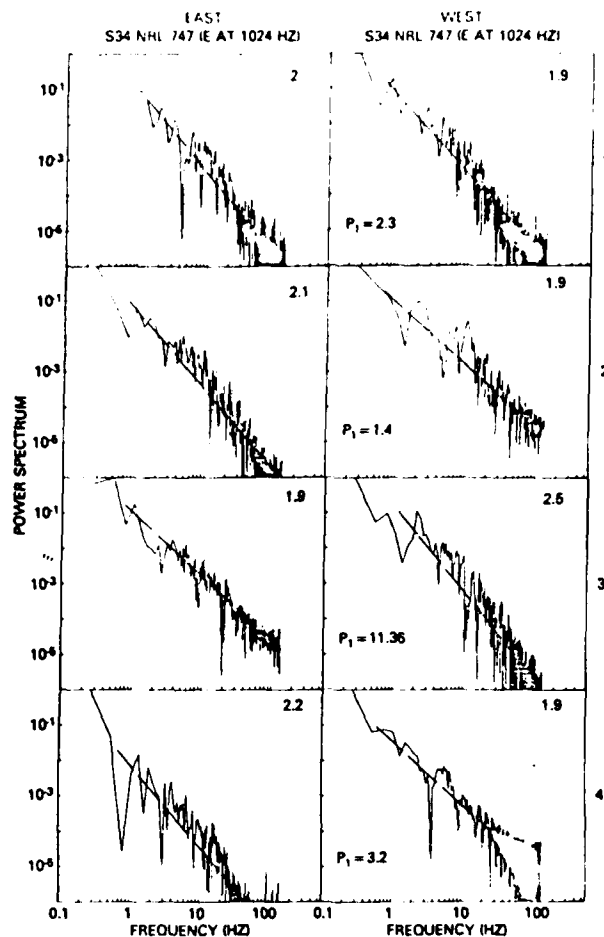


Fig. 4. Power spectral analyses across the boundaries of the four depletions (1-4) in Fig. 3. The number in the upper portion of each panel is the spectral index N , in a $P = P_0 f^{-N}$ fit to the data. The value P_1 shown in each right hand panel corresponds to the ratio of spectral strengths $P_1 = P_0$ (western boundary) \div P_0 (eastern boundary).

the plumes being the more intense. The combined observations support a model of E-W asymmetry which allows for a neutral-wind-driven instability-growth-rate enhancement on the western side of a rising bottomside F -region depletion (Tsunoda, 1979).

4. CONCLUSIONS

The combination of recent rocket and satellite data allows for the development of a two-dimensional empirical model of equatorial depletions and associated irregularities. Elements in the data have led to the following conclusions:

(1) Equatorial depletions are macrostructures within which much smaller scale irregularities are imbedded;

(2) These smaller scale irregularities (in the vertical plane) tend to derive their energies from positive density gradients on the topside of local depletions;

(3) Vertical and horizontal power spectral analyses display indices from 1.8 to 2.5, a result which is consistent with Rayleigh-Taylor instability generation of intermediate wavelength irregularities during the occurrence of equatorial spread- F (Keskinen *et al.* 1980a);

(4) When viewed horizontally, bottomside depletions have an east-west asymmetry with the more intense fluctuations and spectral strengths being observed on the western boundary. This result is consistent with the radar measurements of TSUNODA (1979) and scintillation observations of LIVINGSTON *et al.* (1980);

(5) The combination of all results leads to a two-dimensional model of macroscopic *F*-region depletions with smaller scale structures developing on the top and western boundaries. This model and associated spectral indices fully supports the computational work of KESKINEN *et al.* (1980a).

REFERENCES

- | | | |
|--|-------|---|
| HOLMES J. C. and SZUSZCZEWICZ E. P. | 1975 | <i>Rev. scient. Instrum.</i> 46 , 592. |
| KELLEY M. C., HAERENDAL G., KAPPLER H.,
VALENZUELA A., BALSLEY B. B.,
CARTER D. A., ECKLUND W. L.,
CARSON C. W., HAUSLER B.
and TORBERT R. | 1976 | <i>Geophys. Res. Lett.</i> 3 , 448. |
| KESKINEN M. J., OSSAKOW S. L. and
CHATURVEDI P. K. | 1980a | <i>J. geophys. Res.</i> 85 , 1775. |
| KESKINEN M. J., SZUSZCZEWICZ E. P.,
OSSAKOW S. L. and HOLMES J. C. | 1980b | <i>J. geophys. Res.</i> Submitted. |
| MORSE F. A., EDGAR B. C., KOONS H. C.,
RICE C. J., HEIKKILA W. J.,
HOFFMAN J. H., TINSLEY B. A.,
WINNINGHAM J. D., CHRISTENSEN A. B.,
WOODMAN R. F., PONALAZA J. and
TEIZEIRA N. R. | 1977 | <i>J. geophys. Res.</i> 82 , 578. |
| SCANNAPIECO A. J. and OSSAKOW S. L. | 1976 | <i>Geophys. Res. Lett.</i> 3 , 451. |
| SZUSZCZEWICZ E. P., TSUNODA R. T., NARCISI R.
and HOLMES J. C. | 1980 | <i>Geophys. Res. Lett.</i> 7 , 537. |
| WEBER E. J., BUCHAU J., EATHER R. H.
and MENDE S. B. | 1978 | <i>J. geophys. Res.</i> 83 , 712. |
| WOODMAN R. E. and LA HOZ C. | 1976 | <i>J. geophys. Res.</i> 81 , 5447. |
| <i>Reference is also made to the following unpublished material:</i> | | |
| LIVINGSTON R. C., WEBER E. and BAUCHAU T. | 1980 | Paper presented at International Symposium on
Equatorial Aeronomy, Aguidilla, P.R. |
| SZUSZCZEWICZ E. P. and HOLMES J. C. | 1980 | NRL Memorandum Report 4289. |
| TSUNODA R. T. | 1979 | Topical Report 4, SRI. International. |

SECURITY CLASSIFICATION OF THIS PAGE (When Data Entered)

REPORT DOCUMENTATION PAGE		READ INSTRUCTIONS BEFORE COMPLETING FORM
1. REPORT NUMBER NRL Memorandum Report 4514	2. GOVT ACCESSION NO.	3. RECIPIENT'S CATALOG NUMBER
4. TITLE (and Subtitle) THE STP/S3-4 SATELLITE EXPERIMENT: HIGH LATITUDE LARGE SCALE DENSITY IRREGULARITIES	5. TYPE OF REPORT & PERIOD COVERED Interim report on a continuing NRL problem.	
7. AUTHOR(s) P. Rodriguez, M. Singh*, E. P. Szuszczewicz, D. N. Walker, and J. C. Holmes	6. PERFORMING ORG. REPORT NUMBER	
9. PERFORMING ORGANIZATION NAME AND ADDRESS Naval Research Laboratory Washington, DC 20375	8. CONTRACT OR GRANT NUMBER(s)	
11. CONTROLLING OFFICE NAME AND ADDRESS Office of Naval Research Defense Nuclear Agency Arlington, VA 22217 Washington, DC 20305	10. PROGRAM ELEMENT, PROJECT, TASK AREA & WORK UNIT NUMBERS 61153N; RR033-02-44; 41-0949-0-1	
14. MONITORING AGENCY NAME & ADDRESS (if different from Controlling Office)	12. REPORT DATE May 26, 1981	
	13. NUMBER OF PAGES 26	
	15. SECURITY CLASS. (of this report) UNCLASSIFIED	
	15a. DECLASSIFICATION/DOWNGRADING SCHEDULE	
16. DISTRIBUTION STATEMENT (of this Report) Approved for public release; distribution unlimited.		
17. DISTRIBUTION STATEMENT (of the abstract entered in Block 20, if different from Report)		
18. SUPPLEMENTARY NOTES *Present address: Sachs/Freeman Associates, Inc., Bowie, MD 20715 (On leave from Punjabi University, Patiala, India). This report was partially sponsored by the Defense Nuclear Agency under Subtask I25AAXHX, work unit 00014, work unit title "Nuclear Weapons Effects Program," and the Office of Naval Research.		
19. KEY WORDS (Continue on reverse side if necessary and identify by block number) F-Region irregularities Diffuse aurora Discrete aurora Power spectrum		
20. ABSTRACT (Continue on reverse side if necessary and identify by block number) Large scale density irregularities in the nighttime auroral zone F-region are routinely detected by a pair of pulsed plasma probes on the S3-4 satellite. The absolute density variations can be as large as an order of magnitude and in the case of a quiet diffuse aurora, the irregularities appear to be consistent with the sheet-like structures that have been postulated to explain high latitude scintillation enhancements. In a more dynamic situation, which we believe to be a surging aurora, the density variations may be (Continues)		

DD FORM 1473
1 JAN 73EDITION OF 1 NOV 65 IS OBSOLETE
S/N 0102-014-6601

SECURITY CLASSIFICATION OF THIS PAGE (When Data Entered)

20. ABSTRACT (Continued)

associated with a density gradient and/or current-driven plasma instability. We have made preliminary analyses of the density fluctuations and FFT power spectra for evidence of characteristic scale sizes and power law dependence. Scale sizes from 10-300 km are clearly evident in the irregularities; power law fits to the spectra have spectral indices in the range -1.5 to -1.7. For the diffuse aurora our results suggest support for a recent numerical study of the nonlinear evolution of the current convective instability.

CONTENTS

I. INTRODUCTION	1
II. MEASUREMENTS AND ANALYSIS	1
Plasma Density Measurements	1
Quiescent Aurora	2
Dynamic Aurora	6
III. CONCLUDING COMMENTS	10
ACKNOWLEDGMENTS	11
REFERENCES	11

THE STP/S3-4 SATELLITE EXPERIMENT: HIGH LATITUDE LARGE SCALE DENSITY IRREGULARITIES

INTRODUCTION

The polar regions of the earth's ionosphere are known to exhibit a wide range of plasma kinetic interactions that are very dynamic and complex. The plasma kinetic processes have interaction scale sizes that range from the order of auroral longitudinal dimensions down to particle gyroradii. Although the phenomenology and morphology of auroral processes are well known, the physical mechanisms are not well understood. Plasma density irregularities in the auroral F-region have been detected through ground-based scintillation observations (Aarons, 1973; Fremouw et al., 1977; Buchau et al., 1978; Rino et al., 1978), satellite measurements (McClure and Hanson, 1973; Dyson et al., 1974; Sagalyn et al., 1974; Phelps and Sagalyn, 1976; Clark and Raitt, 1976; Weber and Buchau, 1981), and rocket observations (Kelley et al., 1980). Several physical mechanisms have been suggested to explain the high latitude irregularities. A recent review (Fejer and Kelley, 1980) lists three general sources of the irregularities: 1) particle production (especially by low energy precipitating electrons), 2) electrostatic turbulence, and 3) plasma instabilities. Except in extremely simple situations, it is likely that all three mechanisms will contribute to the spectrum of irregularities.

In this report we will examine two cases of high latitude measurements of electron density irregularities obtained in the nightside auroral F-region with the pulsed plasma probe experiment on the STP/S3-4 satellite. These two cases suggest the importance of plasma instabilities associated with particle precipitation, i.e., field-aligned currents, and illustrate the variety of density irregularities encountered at high latitudes. The first observation we discuss is that associated with a quiescent aurora, in which the structure of density irregularities is relatively well defined on several scale lengths, from 10 km to about 300 km. These scale lengths are significant for some recent theoretical studies on the applicability of the current convective instability in diffuse auroras. The second observation we discuss was obtained during a more dynamic state of the aurora and serves to illustrate some of the complexity associated with possible gradient- and/or current-driven plasma instabilities in discrete auroras.

MEASUREMENTS AND ANALYSIS

Plasma Density Measurements

The polar-orbiting STP/S3-4 satellite is instrumented with a pair of pulsed-plasma-probes that allow high resolution measurements of electron density N_e , temperature T_e , density fluctuation power spectra $P_{N_e}(k)$, plasma potential V_∞ and

Manuscript submitted March 23, 1981.

variations in the mean ion mass $\delta \bar{M}_i / \bar{M}_i$ [Szuszczewicz et al., 1981]. We briefly review the experimental operation only for the particular data mode of interest here. In the low-data-rate mode, the double probe system sampled electron- and ion- saturation currents simultaneously at 100 samples s^{-1} . Under conditions of fixed-payload potential and stable velocity-field and magnetic-field aspect (see e.g., Szuszczewicz and Takacs, 1979), the density N_e and density fluctuation ΔN_e are directly proportional to the probe saturation current I_e and its fluctuations ΔI_e . The STP/S3-4 satellite was in a sun synchronous orbit with an inclination of 96.5° and crossed the equatorial plane at local times of 2230 and 1030. The altitude ranged from 160 to 260 km. In the discussion below of irregularity scale lengths, we will use an average spacecraft velocity of 8 km s^{-1} to convert time variations to spatial variations, using $\Delta L = v \Delta t$, where ΔL is the spatial length, v is the spacecraft velocity, and Δt is the sampled time interval.

Quiescent Aurora

About five minutes of saturation currents, I_e and I_i , obtained on orbit 390 are shown in Figure 1. These measurements were obtained in the night side auroral F-region over the south pole at an altitude of 260 km with the spacecraft moving from the south polar cap region toward the nightside equator (left to right in Figure 1). The probe currents clearly show that irregularities were detected on both electron and ion probes. The detailed tracking of one probe by the other indicates that the probe system was working properly and that the irregularities were due primarily to variations in the ambient electron and ion densities and not the result of secondary effects such as changing spacecraft potential, aspect sensitivity, etc. In this preliminary report, only the electron density irregularities will be discussed, and we simply note the correlative behavior of the ion density irregularities.

The large depletion in electron density (almost an order of magnitude) centered at 1840 UT corresponds to a diffuse aurora. The geomagnetic Kp index for the period of this measurement was 1+, indicating relatively quiescent auroral conditions. The ion density shows a similar depletion. Both the electron and ion depletions extend over a time interval of about 25 s, corresponding to a distance of about 200 km along the approximately south-north direction of spacecraft motion. This aurora was also detected by Huffman et al. (1980) with the vacuum ultraviolet (VUV) experiment on board the same spacecraft. A detailed comparison of the density measurements in Figure 1 with the VUV measurements

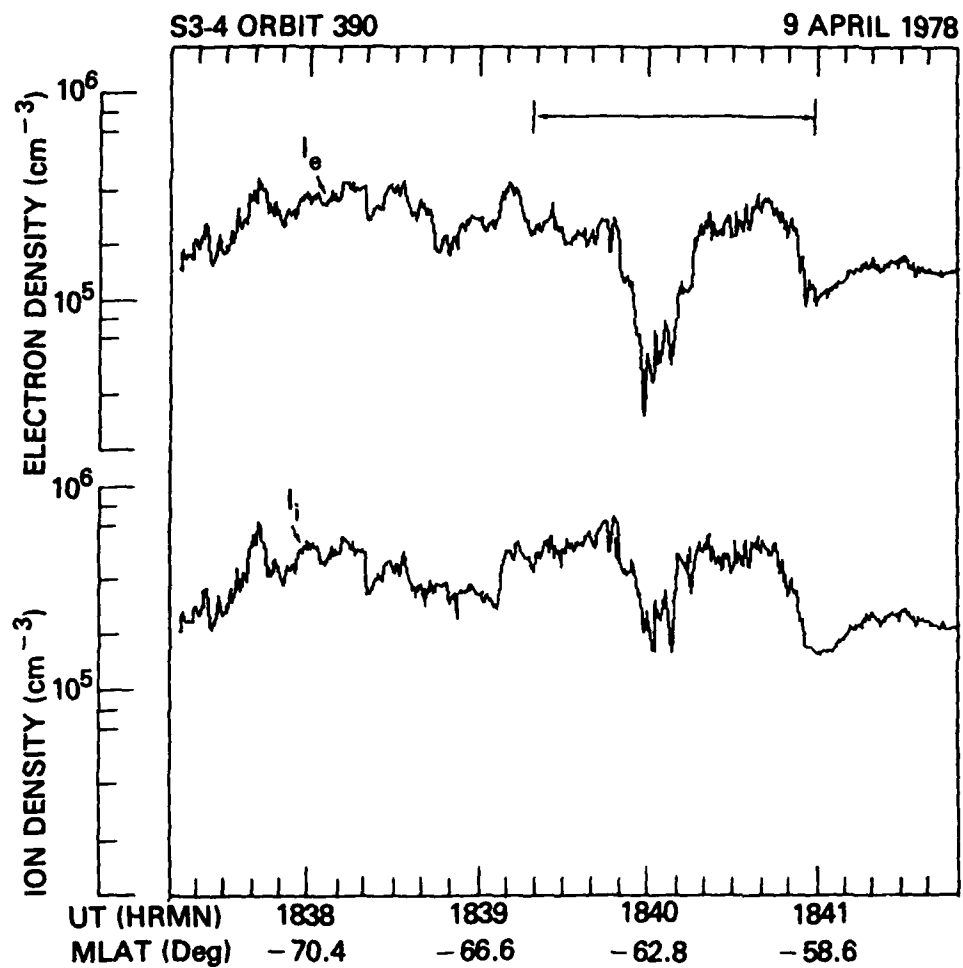


Fig. 1 - The electron and ion currents sampled in the nightside auroral F-region during a pass through a quiescent diffuse aurora.

(Fig. 15 in Huffman et al.) indicates that a good correlation exists. A few discrete arcs detected by the VUV measurement in the time interval 1839-1840 UT appear to be correlated with some of the density structure. Equatorward (to the right) of the large depletion, the electron density shows a relative enhancement with a scale length of about 300 km.

A more detailed plot of the electron density depletion of Figure 1 and its contiguous domains is shown in Figure 2. (The expanded interval is indicated by the arrows above the electron current trace in Figure 1.) In this plot every data point sampled at 100 s^{-1} is shown and the density scale on the left of the figure is approximate. Within the depletion at least three well-defined density variations with nearly periodic behavior are indicated. Assuming the auroral structure to be relatively stable, the width of the three density structures along the spacecraft trajectory is about 20 km and the large scale depletion has a width of about 200 km. On either side of the large scale depletion the density irregularities generally appear to have high and low frequency components with the low frequency components having scale widths comparable to the widths of the density structures within the depletion, i.e., about 20 km.

The Fast Fourier Transform (FFT) power spectrum of the density irregularities in each of three intervals are shown in the insets to Figure 2. The data time interval over which the FFT was calculated is indicated below each spectrum. The Nyquist frequency for each spectrum is 6.25 Hz, corresponding to a minimum scale size of about 0.6 km. Each spectrum is normalized to the maximum power calculated from the FFT. The straight line drawn through each spectrum is the least-squares power law $P = P_0 f^n$, where P/P_0 is the normalized power, f is the frequency, and n is the spectral index. The spectra are calculated without smoothing, except for the removal of the lowest frequency (DC) component by applying a linear detrend.

The first power spectrum (on the left) suggests a k -dependence of $k^{-1.48}$, where $k = 2\pi/\lambda$ is the wave number and λ is the wavelength of the spatial irregularity. The value of the index is consistent with previous reports (Dyson et al., 1974; Sagalyn et al., 1974; Phelps and Sagalyn, 1976; Kelley et al., 1980) on high latitude irregularities where scale sizes from less than 1 km up to 200 km have been considered. In the second power spectrum, taken within the large scale depletion, the spectral index implies a $k^{-1.58}$ variation in spatial irregularity. The low frequency

S3-4 ORBIT 390

NIGHTSIDE AURORAL REGION

9 APRIL 1978

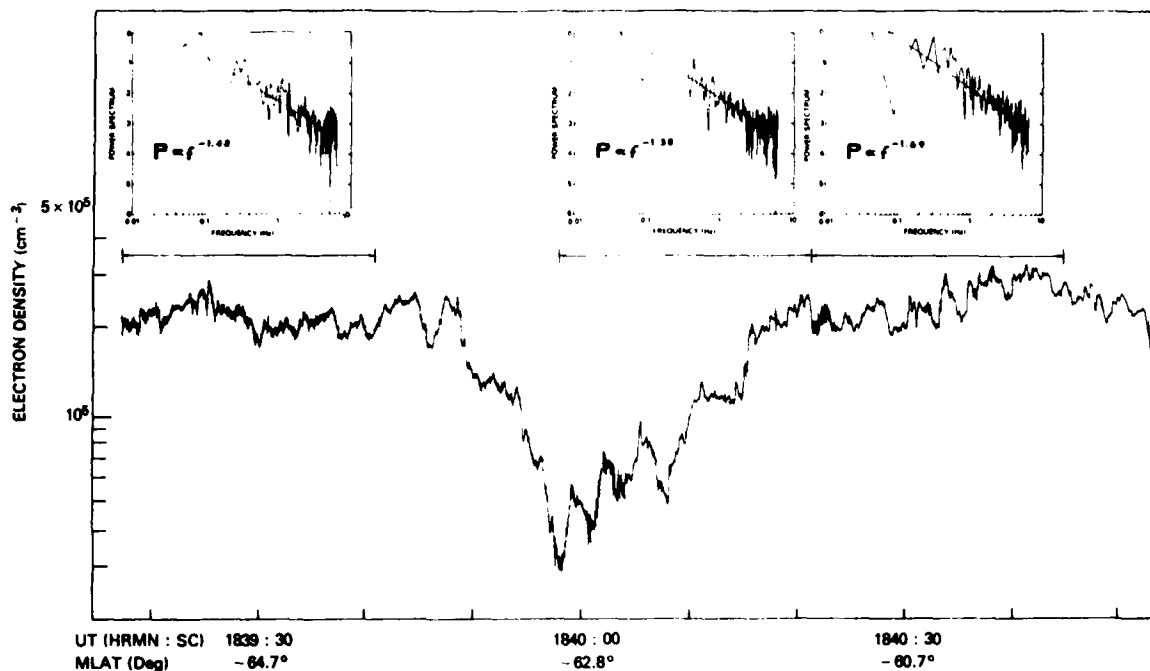


Fig. 2 - An expanded time-scale plot of electron density irregularities in the diffuse aurora of Figure 1. The power spectra indicate the frequency dependence of the least-squares power law. Frequency f is directly proportional to wave-number k , assuming the irregularities are spatial structures.

spectral range 0.1-0.3 Hz corresponds to the well-defined structures of about 20 km half-width in the density-vs-time plot. The spectral power in the 20-km structures inside the large density depletion is about three times greater than the power in similar scale size structures outside the depletion, a fact not obvious in the power spectra because of the normalization. The third power spectrum shows a power law dependence with a spectral index of -1.69.

An examination of the density-vs-time plot of Figure 2 shows that approximately 20-km scale size structures are clearly evident both inside and outside the large depletion. A possible source of these 20-km density irregularities is suggested by recent theoretical studies on the current convective instability in diffuse auroras (Ossakow and Chaturvedi, 1979; Keskinen et al., 1980; Huba and Ossakow, 1980). The current convective instability is proposed as a mechanism for generating large scale (~ 10 -50 km) density irregularities in the diffuse auroral F-region. The current convective instability may thus provide an explanation for the sheet-like density irregularities that have been detected by Fremouw et al. (1977) and Rino et al. (1978) in their analysis of enhanced scintillations at auroral latitudes. In a numerical analysis, Keskinen et al., (1980) considered the nonlinear evolution of the current convective instability with an initial density gradient scale size of 50 km. They obtained a spectrum of irregularities with a spectral index of -1.7 in the north-south direction. This scale size and spectral index are similar to the scale lengths and to the spectral indices shown in Figure 2. Thus we suggest that the observations provide experimental support for the current convective instability as a possible mechanism for the density irregularities associated with the diffuse aurora.

Dynamic Aurora

The plasma probe measurements of Figure 3 illustrate the case of a dynamic aurora observed on orbit 244 in the southern night-side auroral F-region. The K_p index for this period was 3+, indicating that moderately active geomagnetic perturbations were occurring. As in Figure 1, the electron and ion saturation currents were sampled in the low-data-rate mode (100 s^{-1}). The two currents track each other very well so that we are confident of proper measurements directly proportional to the ambient plasma density. The outstanding features of the density measurements in Figure 3 are the sharp transition in density occurring at about

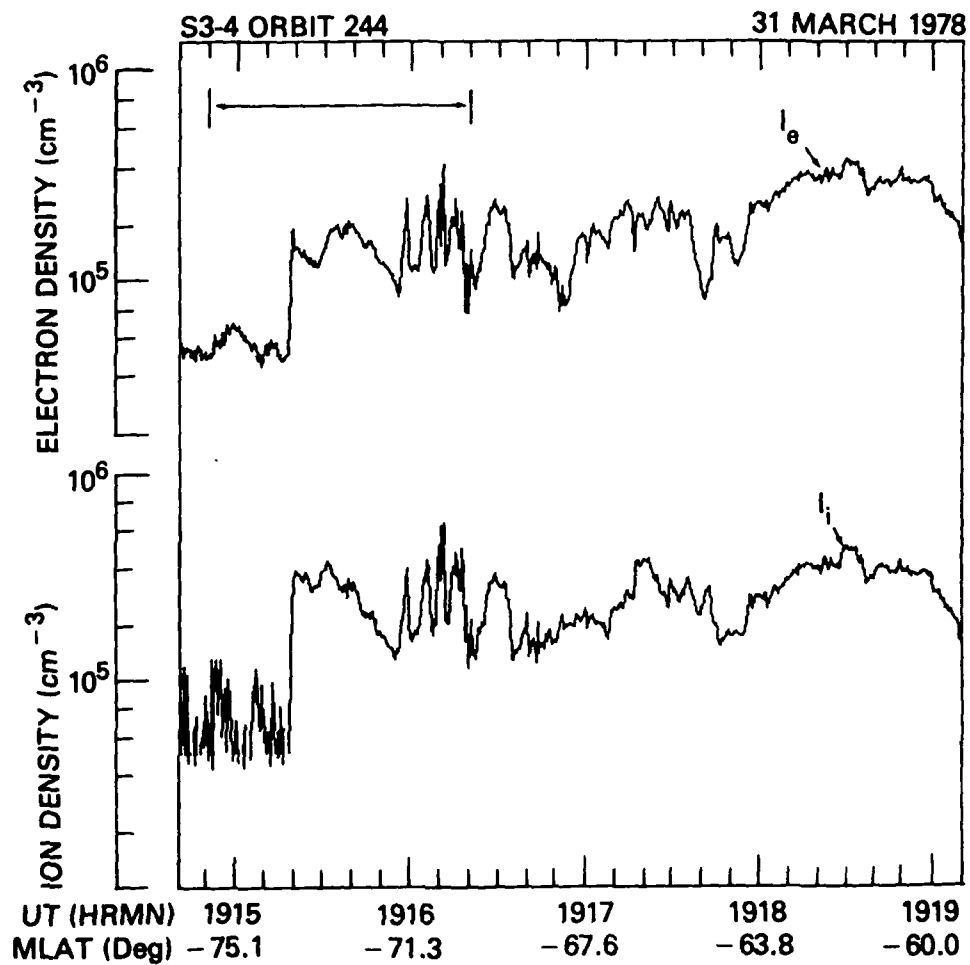


Fig. 3 - The electron and ion currents sampled in the nightside auroral F-region for a dynamic state of the aurora.

1915:15 UT and the large peak-to-peak variations between 1916 and 1917 UT. The sharp transition in density is more apparent in the electron current than in the ion current because of noise interference occurring in the ion probe before about 1915:10 UT. A detailed comparison of the two currents shows that the transition itself is unaffected by the noise and the two currents track each other almost exactly within the transition.

A detailed plot of the electron current in the time interval indicated by the arrows in Figure 3 is shown in Figure 4 with an approximate density scale to the left. The sharp transition begins at about 1915:17 UT and consists of large irregular oscillations over the transition width of about 1.5 s. The density jump associated with the transition is about a factor of 4. Immediately behind the transition there are at least four distinct oscillations with an average period of about 2 s. These oscillations seem to decay exponentially, as indicated by the dashed line (on a log scale, an exponential curve will appear as a straight line). The VUV observations on the same spacecraft indicate that auroral emissions were detected at the same time the density transition occurred (R.E. Huffman, private communication) suggesting that the density jump is associated with a discrete auroral arc. The observation of a sharp transition suggests that a moving boundary has been detected and we conclude that the density jump is associated with the surge of an auroral arc. The surge direction cannot actually be determined from our observations; generally the movement is westward and poleward (Akasofu, 1968). The sharp transition in density implies that gradient-driven plasma instabilities are likely to occur; with our interpretation of a surging auroral arc, the decaying oscillations behind the density jump would represent spatial oscillations left behind by the movement of the source of instability, the surge front. The electron density increase by a factor of 4 across the surge front probably results from the enhanced ionization due to precipitating particles. Similar ionization enhancements of the F-layer associated with discrete auroral arcs have been observed with ionospheric sounders (Pike et al., 1977). The surge front very likely has field-aligned currents associated with it (Iijima and Potemra, 1978), so that current-driven plasma instabilities are also likely to be present and may contribute to the density oscillations. It is possible that the large and irregular variations seen at later times (after 1915:55 UT) also may have had their origin in the surge of the auroral arc. If the irregular density structures behind the surge front are quasi-stationary, then a wide range of scale lengths is evident, from about 4 km to 70 km and longer. In contrast, the region ahead of the surge

S3-4 ORBIT 244

NIGHTSIDE AURORAL REGION

31 MARCH 1978

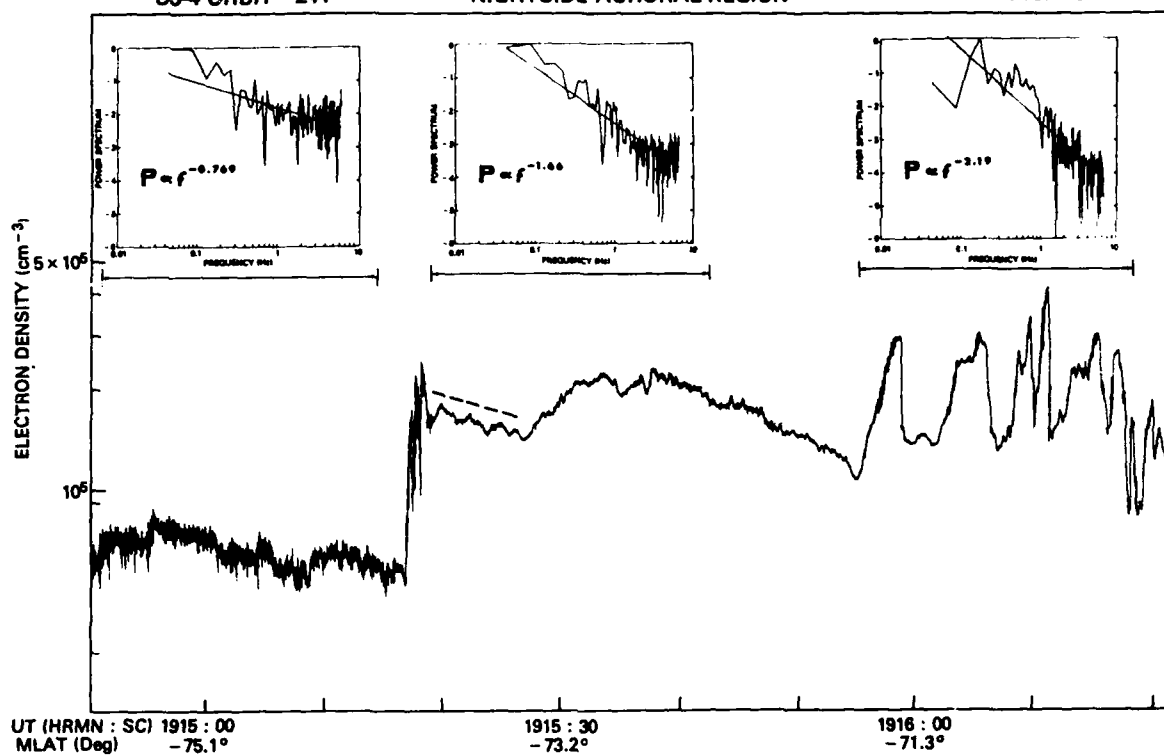


Fig. 4 - An expanded time-scale plot of the electron density for the aurora of Figure 3. The sharp density jump is identified as the surge of a discrete auroral arc. An exponential decay for the well-defined oscillations behind the surge front is suggested by the dashed line.

front has a distinctly different appearance, with only low amplitude, high frequency variations. This region ahead of the surge front may be a relatively quiescent ionosphere about to be perturbed by the surging auroral arc. The different character of the irregularities on either side of the density jump that we have identified as a surging auroral arc is additional evidence that the density jump is a dynamic transition between two states of the F-region ionosphere.

The power spectra for three time intervals are also shown in Figure 4. Just ahead of the density jump the spectrum of the irregularities shows that the slope of the least-squares power law is relatively flat, suggesting that thermal fluctuations dominate the spectrum and the ionosphere is in a quiescent state. The spectrum immediately behind the density jump shows a power law with steeper slope, indicating the presence of enhanced power at low frequencies. The well-defined decaying oscillations behind the density jump appear in the spectrum as the component centered on a frequency of about 0.3 Hz. Under the assumption that they are spatial variations, these oscillations have a scale length of about 10 km. The spectral index $n = -1.66$ for the second spectrum in Figure 4 is nearly identical to one of the spectra in Figure 2. This near-equality suggests that similar transfer processes in spectral energy may be involved. (We note, however, that a specific spectral index does not uniquely define an instability process.) The third spectrum in Figure 4 corresponds to the region of large peak-to-peak variations. The spectrum clearly shows the predominance of structure in the range 0.1-1.0 Hz (40-4 km). The spectral index is near -2, possibly due to the presence of steep edges in the irregularities.

CONCLUDING COMMENTS

The aurora-related F-region density irregularities discussed in this report illustrate the variety of plasma kinetic processes that are involved in high latitude ionospheric effects. Our study of the density irregularities is in a preliminary stage, and we expect that new and significant results will be forthcoming as the study advances. It is already obvious from an initial survey of available satellite data that aurora-related effects are detected outside the average auroral boundaries, i.e., both at higher and lower latitudes. Since the high latitude region is directly associated with magnetosphere-ionosphere coupling processes, we anticipate that the analysis of the ionospheric density irregularities in regions such as the polar cusp will address problems of global importance.

ACKNOWLEDGMENT

The authors wish to thank the Air Force Space Test Program, the Naval Space Systems Activity and the Office of Naval Research for support throughout this program. We are also indebted to Messrs. Swinney and Kegley for their diligent efforts in all phases of fabrication, testing and integration. This work was supported within the Ionospheric and Stratospheric Task Area (0949-0) and conducted within the Ionospheric Diagnostics Section of the Space Science Division.

REFERENCES

- Aarons, J., "A descriptive model of F-layer high-latitude irregularities as shown by scintillation observations", *J. Geophys. Res.*, 78, 7441 (1973).
- Akasofu, S.-I., "Polar and magnetospheric substorms", Springer, New York (1968).
- Buchau, J., J. Aarons, J.P. Mullen, E.J. Weber, J.A. Whalen, H.E. Whitney and E.E. Crampton, "Amplitude scintillation studies in the polar region on 250 MHz", in Effects of the Ionosphere on Space and Terrestrial Systems, edited by J.M. Goodman, U.S. Government Printing Office, Washington, DC (1978).
- Clark, D.H., and W.J. Rait, "The global morphology of irregularities in the topside ionosphere as measured by the total ion current probe on ESRO-4", *Planet. Space Sci.*, 24, 873 (1976).
- Dyson, P.L., J.P. McClure and W.B. Hanson, "In situ measurements of the spectral characteristics of F-region ionospheric irregularities", *J. Geophys. Res.*, 79, 1497, (1974).
- Fejer, B.G. and M.C. Kelley, "Ionospheric irregularities", *Rev. Geophys. Sp. Phys.*, 18, 401 (1980).
- Fremouw, E.J., C.L. Rino, R.C. Livingston and M.C. Cousins, "A persistent subauroral scintillation enhancement observed in Alaska", *Geophys. Res. Lett.* 4, 539 (1977).
- Holmes, J.C. and E.P. Szuszczewicz, "A versatile plasma probe", *Rev. Sci. Instr.*, 46, 592 (1975).
- Huba, J.D. and S.L. Ossakow, "Influence of magnetic shear on the current convective instability in the diffuse aurora", *J. Geophys. Res.*, 85, 6874 (1980).

- Huffman, R.E., F.J. LeBlanc, J.C. Larrabee and D.E. Paulsen, "Satellite vacuum ultraviolet airglow and auroral observations", J. Geophys. Res. 85, 2201 (1980).
- Iijima, T., and T. A. Potemra, "Large-scale characteristics of field-aligned currents associated with substorms", J. Geophys. Res., 83, 599 (1978).
- Kelley, M.C., K.D. Baker, J.C. Ulwick, C.L. Rino and M.J. Baron, "Simultaneous rocket probe, scintillation, and incoherent scatter radar observations of irregularities in the auroral zone ionosphere", Radio Sci., 15, 491 (1980).
- Keskinen, M.J., S.L. Ossakow and B.E. McDonald, "Nonlinear evolution of diffuse auroral F-region ionospheric irregularities", Geophys. Res. Lett., 7, 573 (1980).
- McClure, J.P. and W.B. Hanson, "A catalog of ionospheric F-region irregularity behavior based on OGO 6 retarding potential analyzer data", J. Geophys. Res., 78, 7431 (1973).
- Ossakow, S.L. and P.K. Chaturvedi, "Current convective instability in the diffuse aurora", Geophys. Res. Lett., 6, 332 (1979).
- Phelps, A.D.R., and R.C. Sagalyn, "Plasma density irregularities in the high-latitude topside ionosphere", J. Geophys. Res., 81, 515 (1976).
- Pike, C.P., J.A. Whalen and J. Buchau, "A 12-hour case study of auroral phenomena in the midnight sector: F-layer and 6300-A measurements", J. Geophys. Res., 82, 3547 (1977).
- Rino, C.L., R.C. Livingston and S.J. Mathews, "Evidence for sheet-like auroral ionospheric irregularities", Geophys. Res. Lett., 5, 1039 (1978).
- Sagalyn, R.C., M. Smiddy, and M. Ahmed, "High-latitude irregularities in the topside ionosphere based on ISIS 1 thermal ion probe", J. Geophys. Res., 79, 4252 (1974).
- Szuszczewicz, E.P. and P. Z. Takacs, "Magnetosheath effects on cylindrical Langmuir probes", Phys. Fluids, 22, 2424 (1979).
- Szuszczewicz, E.P. and J.C. Holmes, "The STP/S3-4 ionospheric irregularities satellite experiment", J. Geophys. Res., (submitted, 1981).
- Weber, E.J. and J. Buchau, "Polar cap F-layer auroras", Geophys. Res. Lett., 8, 125 (1981).

DISTRIBUTION LIST

DEPARTMENT OF DEFENSE

ASSISTANT SECRETARY OF DEFENSE
COMM, DMD, CONT & INTELL
WASHINGTON, D.C. 20301
O1CY ATTN J. BABCOCK
O1CY ATTN M. EPSTEIN

DIRECTOR
COMMAND CONTROL TECHNICAL CENTER
PENTAGON RM BE 685
WASHINGTON, D.C. 20301
O1CY ATTN C-650
O1CY ATTN C-312 R. MASON

DIRECTOR
DEFENSE ADVANCED RSCH PROJ AGENCY
ARCHITECT BUILDING
1400 WILSON BLVD.
ARLINGTON, VA. 22209
O1CY ATTN NUCLEAR MONITORING RESEARCH
O1CY ATTN STRATEGIC TECH OFFICE

DEFENSE COMMUNICATION ENGINEER CENTER
1860 WIEHLE AVENUE
RESTON, VA. 22290
O1CY ATTN CODE R820
O1CY ATTN CODE R410 JAMES W. MCLEAN
O1CY ATTN CODE R720 J. WORTHINGTON

DEPT. OF THE AIR FORCE
HEADQUARTERS SPACE DIVISION
(AFSC) LOS ANGELES AIR FORCE STATION
P.O. BOX 92960
LOS ANGELES, CA 90009
O1CY DIRECTOR, STP,
COL D.E. THURSBY
O1CY MAJ C. JUND

DIRECTOR
DEFENSE INTELLIGENCE AGENCY
WASHINGTON, D.C. 20301
O1CY ATTN DT-18
O1CY ATTN DB-4C E. O'FARRELL
O1CY ATTN DIAAP A. WISE
O1CY ATTN DIAST-5
O1CY ATTN DT-1BZ R. MORTON
O1CY ATTN HQ #1-TR J. STEWART
O1CY ATTN W. WITTIG DC-7D

DIRECTOR
DEFENSE NUCLEAR AGENCY
WASHINGTON, D.C. 20305
O1CY ATTN STVL
O4CY ATTN TITL
O1CY ATTN DDST
O3CY ATTN RAAE

COMMANDER
FIELD COMMAND
DEFENSE NUCLEAR AGENCY
KIRTLAND AFB, NM 87115
O1CY ATTN FCPR

DIRECTOR
INTERSERVICE NUCLEAR WEAPONS SCHOOL
KIRTLAND AFB, NM 87115
O1CY ATTN FCPR

DIRECTOR
JOINT STRAT TGT PLANNING STAFF
OFFUTT AFB
OMAHA, NB 68113
O1CY ATTN JLTW-2
O1CY ATTN JPST G. GOETZ

JOINT CHIEFS OF STAFF
WASHINGTON, D.C. 20301
O1CY ATTN J-3 WWMCCS EVALUATION
OFFICE

CHIEF
LIVERMORE DIVISION FLD COMMAND DNA
DEPARTMENT OF DEFENSE
LAWRENCE LIVERMORE LABORATORY
P.O. BOX 808
LIVERMORE, CA 94550
O1CY ATTN FCPR

DIRECTOR
NATIONAL SECURITY AGENCY
DEPARTMENT OF DEFENSE
FT. GEORGE G. MEADE, MD 20755
O1CY ATTN JOHN SKILLMAN R52
O1CY ATTN FRANK LEONARD
O1CY ATTN W14 FAT CLARK
O1CY ATTN OLIVER H. BARTLETT W32
O1CY ATTN R5

COMMANDANT
NATO SCHOOL (SHAPE)
APO NEW YORK 09172
O1CY ATTN U.S. DOCUMENTS OFFICER

UNDER SECY OF DEF FOR RSCH & ENGR.
DEPARTMENT OF DEFENSE
WASHINGTON, D.D. 20301
O1CY ATTN STRATEGIC & SPACE SYSTEMS
(OS)

COMMANDER
U.S. ARMY COMM-ELEC ENGRG INSTAL AGY
FT. HUACHUCA, AZ 85613
O1CY ATTN CCC-EMEO GEORGE LANE

WMCCS SYSTEM ENGINEERING ORG.
WASHINGTON, D.C. 20305
O1CY ATTN R. CRAWFORD

COMMANDER/DIRECTOR
ATMOSPHERIC SCIENCES LABORATORY
U.S. ARMY ELECTRONICS COMMAND
WHITE SANDS MISSILE RANGE, NM 88002
O1CY ATTN DELAS-EO F. NILES

DIRECTOR
BMD ADVANCED TECH CTR
HUNTSVILLE OFFICE
P.O. BOX 1500
HUNTSVILLE, AL 35807
O1CY ATTN ATC-T MELVIN T. CAPPS
O1CY ATTN ATC-O W. DAVIES
O1CY ATTN ATC-R DON RUSS

PROGRAM MANAGER
BMD PROGRAM OFFICE
5001 EISENHOWER AVENUE
ALEXANDRIA, VA 22333
O1CY ATTN DACS-BMT J. SHEA

CHIEF C-E SERVICE DIVISION
U.S. ARMY COMMUNICATIONS CMD
PENTAGON RM. 1B269
WASHINGTON, D.C. 20310
O1CY ATTN C-E-SERVICES DIVISION

COMMANDER
FRADCOM TECHNICAL SUPPORT ACTIVITY
DEPARTMENT OF THE ARMY
FORT MONMOUTH, N.J. 07703
O1CY ATTN DRSEL-NL-RD H. BENNET
O1CY ATTN DRSEL-PL-ENV H. BOMKE
O1CY ATTN J.E. QUIGELY

COMMANDER
HARRY DIAMOND LABORATORIES
DEPARTMENT OF THE ARMY
2800 POWDER MILL ROAD
ADELPHI, MD 20783
(CNWDI-INNER ENVELOPE: ATTN: DELHD-RBH)
O1CY ATTN DELHD-TI M. WEINER
O1CY ATTN DELHD-RB R. WILLIAMS
O1CY ATTN DELHD-NP F. WIMENITZ
O1CY ATTN DELHD-NP C. MOAZED

COMMANDER
U.S. ARMY COMM-ELEC ENGRG INSTAL AGY
FT. HUACHUCA, AZ 85613
O1CY ATTN CCC-EMEO GEORGE LANE

COMMANDER
U.S. ARMY FOREIGN SCIENCE & TECH CTR
220 7TH STREET, NE
CHARLOTTESVILLE, VA 22901
O1CY ATTN DRXST-SD
O1CY ATTN R. JONES

COMMANDER
U.S. ARMY MATERIAL DEV & READINESS CMD
5001 EISENHOWER AVENUE
ALEXANDRIA, VA 22333
O1CY ATTN DRCLDC J.A. BENDER

COMMANDER
U.S. ARMY NUCLEAR AND CHEMICAL AGENCY
7500 BACKLICK ROAD
BLDG. 2073
SPRINGFIELD, VA 22150
O1CY ATTN LIBRARY

DIRECTOR
U.S. ARMY BALLISTIC RESEARCH LABS
ABERDEEN PROVING GROUND, MD 21005
O1CY ATTN TECH LIB EDWARD BAICY

COMMANDER
U.S. ARMY SATCOM AGENCY
FT. MONMOUTH, NJ 07703
O1CY ATTN DOCUMENT CONTROL

COMMANDER
U.S. ARMY MISSILE INTELLIGENCE AGENCY
REDSTONE ARSENAL, AL 35809
O1CY ATTN JIM GAMBLE

DIRECTOR
U.S. ARMY TRADOC SYSTEMS ANALYSIS ACTIVITY
WHITE SANDS MISSILE RANGE, NM 88002
O1CY ATTN ATAA-SA
O1CY ATTN TCC/F. PAYAN JR.
O1CY ATTN ATAA-TAC LTC. J. HESSE

COMMANDER
NAVAL ELECTRONIC SYSTEMS COMMAND
WASHINGTON, D.C. 20360
O1CY ATTN NAVLEX 034 T. HUGHES
O1CY ATTN PME 117
O1CY ATTN PME 117-T
O1CY ATTN CODE 5011
O1CY ATTN PME-106-T

COMMANDING OFFICER
NAVAL INTELLIGENCE SUPPORT CTR
4301 SUITLAND ROAD, BLDG. 5
WASHINGTON, D.C. 20390
O1CY ATTN MR. DUBBIN STIC 12
O1CY ATTN NISC-50
O1CY ATTN CODE 5404 J. GALET

COMMANDER
NAVAL SURFACE WEAPONS CENTER
DAHLGREN LABORATORY
DAHLGREN, VA 22448
O1CY ATTN CODE DF-14 R. BUTLER

OFFICE OF NAVAL RESEARCH
ARLINGTON, VA 22217
O1CY ATTN CODE 465
O1CY ATTN CODE 461
O1CY ATTN CODE 420
O1CY ATTN CODE 421

COMMANDER
AEROSPACE DEFENSE COMMAND/DC
DEPARTMENT OF THE AIR FORCE
ENT AFB, CO 80912
O1CY ATTN DC MR. LONG

COMMANDER
AEROSPACE DEFENSE COMMAND/XPD
DEPARTMENT OF THE AIR FORCE
ENT AFB, CO 80912
O1CY ATTN XPDQ
O1CY ATTN XP

AIR FORCE GEOPHYSICS LABORATORY
HANSCOM AFB, MA 01731
O1CY ATTN OPR HAROLD GARDNER
O1CY ATTN OPR-1 JAMES C. ULWICK
O1CY ATTN LKB KENNETH S. W. CAMPION
O1CY ATTN OPR ALVA T. STAIR
O1CY ATTN PHD JURGEN BUCHAU
O1CY ATTN PHD JOHN P. MULLEN

AF WEAPONS LABORATORY
KIRTLAND AFB, NM 87117
O1CY ATTN SUL
O1CY ATTN CA AUTHER H. GUENTHER
O1CY ATTN NYTC CAPT. J. BARRY
O1CY ATTN NYTC JOHN M. KAMM
O1CY ATTN NYTC CAPT MARK A. FRY
O1CY ATTN NTES MAJ GARY GANONG
O1CY ATTN NYTC J. JANNI

AFTAX
PATRICK AFB, FL 32925
O1CY ATTN TF/MAJ WILEY
O1CY ATTN TN

AIR FORCE WRIGHT AERONAUTICAL LABS
WRIGHT-PATTERSON AFB, OH 45433
O1CY ATTN AAAD, WADE HUNT
O1CY ATTN AAAD, ALLEN JOHNSON

DEPUTY CHIEF OF STAFF
RESEARCH, DEVELOPMENT, & ACQ
DEPARTMENT OF THE AIR FORCE
WASHINGTON, D.C. 20330
O1CY ATTN AFRDQ

HEADQUARTERS
ELECTRONIC SYSTEMS DIVISION/XR
DEPARTMENT OF THE AIR FORCE
HANSCOM AFB, MA 01731
O1CY ATTN XR J. DEAS

HEADQUARTERS
ELECTRONIC SYSTEMS DIVISION/YSEA
DEPARTMENT OF THE AIR FORCE
HANSCOM AFB, MA 01731
O1CY ATTN YSEA

COMMANDER
NAVAL OCEAN SYSTEMS CENTER
SAN DIEGO, CA 92152
O3CY ATTN CODE 532 W. MOLER
O1CY ATTN CODE 0230 C. BAGGETT
O1CY ATTN CODE 81 R. EASTMAN
O1CY ATTN CODE 2200 H. RICHTER

DIRECTOR
NAVAL RESEARCH LABORATORY
WASHINGTON, D.C. 20375
O1CY CODE 4100
O1CY CODE 4101
O1CY CODE 4120
O1CY CODE 4701 JACK D. BROWN
20CY CODE 2628
O1CY CODE 4732 E. MCLEAN
O1CY CODE 6000
O1CY CODE 7000
O1CY CODE 7500
O1CY CODE 7580
O1CY CODE 7551
O1CY CODE 7555
O1CY CODE 7900

COMMANDER
NAVAL SEA SYSTEMS COMMAND
WASHINGTON, D.C. 20362
O1CY ATTN CAPT. R. PITKIN

COMMANDER
NAVAL SPACE SURVEILLANCE SYSTEM
DAHLGREN, VA 22448
O1CY ATTN CAPT. J.H. BURTON

OFFICER-IN-CHARGE
NAL SURFACE WEAPONS CENTER
WHITE OAK, SILVER SPRING, MD 20910
O1CY ATTN CODE F31

DIRECTOR STRATEGIC SYSTEMS PROJECT OFFICE
DEPARTMENT OF THE NAVY
WASHINGTON, D.C. 20376
O1CY ATTN NSP-2141
O1CY ATTN NSSP-2722 FRED WIMBERLY

NAVAL SPACE SYSTEM ACTIVITY
P.O. BOX 92960
WORLDWAY POSTAL CENTER
LOS ANGELES, CA 90009
O1CY ATTN LCDR DONALD SNODDY
O1CY ATTN COMMANDING OFFICER

HEADQUARTERS
ELECTRONIC SYSTEMS DIVISION/DC
DEPARTMENT OF THE AIR FORCE
HANSCOM AFB, MA 01731
O1CY ATTN DCKC MAJ J.C. CLARK

COMMANDER
FOREIGN TECHNOLOGY DIVISION, AFSC
WRIGHT-PATTERSON AFB, OH 45433
O1CY ATTN NICD LIBRARY
O1CY ATTN ETDP B. BALLARD

COMMANDER
ROME AIR DEVELOPMENT CENTER, AFSC
GRIFFISS AFB, NY 13441
O1CY ATTN DOC LIBRARY/TSLD
O1CY ATTN OCSE V. COYNE

SAMSO/SZ
POST OFFICE BOX 92960
WORLDWAY POSTAL CENTER
LOS ANGELES, CA 90009
(SPACE DEFENSE SYSTEMS)
O1CY ATTN SZJ

STRATEGIC AIR COMMAND/XPFS
OFFUTT AFB, NB 68113
O1CY ATTN XPFS MAJ. B. STEPHAN
O1CY ATTN ADWATE MAJ. BRUCE BAUER
O1CY ATTN NRT
O1CY ATTN DOK CHIEF SCIENTIST

SAMSO/YA.
P.O. BOX 92960
WORLDWAY POSTAL CENTER
LOS ANGELES, CA 90009
O1CY ATTN YAT CAPT L. BLACKWELDER

SAMSO/SK
P.O. BOX 92960
WORLDWAY POSTAL CENTER
LOS ANGELES, CA 90009
O1CY ATTN SKA (SPACE COMO SYSTEMS)
M. CLAVIN

SAMSO/MN
NORTON AFB, CA 92409
(MINUTEMAN)
O1CY ATTN MNML LTC KENNGDY

COMMANDER
ROME AIR DEVELOPMENT CENTER, AFSC
HANSCOM AFB, MA 01731
O1CY ATTN EEP A. LORENTZEN

DEPARTMENT OF ENERGY

DEPARTMENT OF ENERGY
ALBUQUERQUE OPERATIONS OFFICE
P.O. BOX 5400
ALBUQUERQUE, NM 87115
OICY ATTN DOC CON FOR D. SHERWOOD

DEPARTMENT OF ENERGY
LIBRARY ROOM G-042
WASHINGTON, D.C. 20545
OICY ATTN DOC CON FOR A. LABOWITZ

EG&G, INC.
LOS ALAMOS DIVISION
P.O. BOX 809
LOS ALAMOS, NM 85544
OICY ATTN DOC CON FOR J. BREEDLOVE

UNIVERSITY OF CALIFORNIA
LAWRENCE LIVERMORE LABORATORY
P.O. BOX 808
LIVERMORE, CA 94550
OICY ATTN DOC CON FOR TECH INFO DEPT
OICY ATTN DOC CON FOR L-389 R. OTT
OICY ATTN DOC CON FOR L-31 R. HAGER
OICY ATTN DOC CON FOR L-46 F. SEWARD

LOS ALAMOS SCIENTIFIC LABORATORY
P.O. BOX 1663
LOS ALAMOS, NM 87545
OICY ATTN DOC CON FOR J. WOLCOTT
OICY ATTN DOC CON FOR R.F. TASCHEK
OICY ATTN DOC CON FOR E. JONES
OICY ATTN DOC CON FOR J. MALIK
OICY ATTN DOC CON FOR R. JEFFRIES
OICY ATTN DOC CON FOR J. ZINN
OICY ATTN DOC CON FOR P. KEATON
OICY ATTN DOC CON FOR D. WESTERVELT
OICY ATTN DOC CON FOR M. PONGRATZ

SANDIA LABORATORIES
P.O. BOX 5800
ALBUQUERQUE, NM 87115
OICY ATTN DOC CON FOR J. MARTIN
OICY ATTN DOC CON FOR W. BROWN
OICY ATTN DOC CON FOR A. THORNBROUGH
OICY ATTN DOC CON FOR T. WRIGHT
OICY ATTN DOC CON FOR D. DAHLGREN
OICY ATTN DOC CON FOR 3141
OICY ATTN DOC CON FOR SPACE PROJECT DIV

SANDIA LABORATORIES
LIVERMORE LABORATORY
P.O. BOX 969
LIVERMORE, CA 94550
OICY ATTN DOC CON FOR B. MURPHY
OICY ATTN DOC CON FOR T. COOK

OFFICE OF MILITARY APPLICATION
DEPARTMENT OF ENERGY
WASHINGTON, D.C. 20545
OICY ATTN DOC CON FOR D. GALE

OTHER GOVERNMENT

CENTRAL INTELLIGENCE AGENCY
ATTN RD/SI, RM 5G48, HQ BLDG
WASHINGTON, D.C. 20505
OICY ATTN OSI/PSID RM 5F 19

DEPARTMENT OF COMMERCE
NATIONAL BUREAU OF STANDARDS
WASHINGTON, D.C. 20234
(ALL CORRES: ATTN SEC OFFICER FOR)
OICY ATTN R. MOORE

DEPARTMENT OF TRANSPORTATION
OFFICE OF THE SECRETARY
TAD-44.1, ROOM 10402-B
400 7TH STREET, S.W.
WASHINGTON, D.C. 20590
OICY ATTN R. LEWIS
OICY ATTN R. DOHERTY

INSTITUTE FOR TELECOM SCIENCES
NATIONAL TELECOMMUNICATIONS & INFO ADMIN
BOULDER, CO 80303
OICY ATTN A. JEAN (UNCLASS ONLY)
OICY ATTN W. UTLAUT
OICY ATTN D. CROMBIE
OICY ATTN L. BERRY

NATIONAL OCEANIC & ATMOSPHERIC ADMIN
ENVIRONMENTAL RESEARCH LABORATORIES
DEPARTMENT OF COMMERCE
BOULDER, CO 80302
OICY ATTN R. GRUBB
OICY ATTN AERONOMY LAB G. REID

DEPARTMENT OF DEFENSE CONTRACTORS

AEROSPACE CORPORATION

P.O. BOX 92957

LOS ANGELES, CA 90009

OICY ATTN I. GARFUNKEL

OICY ATTN T. SALMI

OICY ATTN V. JOSEPHSON

OICY ATTN S. BOWER

OICY ATTN N. STOCKWELL

OICY ATTN D. OLSEN

OICY ATTN J. CARTER

OICY ATTN F. MORSE

OICY ATTN SMFA FOR PW

OICY ATTN J. FENNEL

OICY ATTN C. RICE

OICY ATTN H. KOONS

ANALYTICAL SYSTEMS ENGINEERING CORP

5 OLD CONCORD ROAD

BURLINGTON, MA 01803

OICY ATTN RADIO SCIENCES

BERKELEY RESEARCH ASSOCIATES, INC.

P.O. BOX 983

BERKELEY, CA 94701

OICY ATTN J. WORKMAN

BOEING COMPANY, THE

P.O. BOX 3707

SEATTLE, WA 98124

OICY ATTN G. KEISTER

OICY ATTN D. MURRAY

OICY ATTN G. HALL

OICY ATTN J. KENNEY

CALIFORNIA AT SAN DIEGO, UNIV OF

IPAPS, 8-019

LA JOLLA, CA 92093

OICY ATTN HENRY G. BOOKER

OICY ATTN E.C. WHIPPLE

BROWN ENGINEERING COMPANY, INC.

CUMMINGS RESEARCH PARK

HUNTSVILLE, AL 35807

OICY ATTN ROMEO A. DELIBERIS

CHARLES STARK DRAPER LABORATORY, INC.

555 TECHNOLOGY SQUARE

CAMBRIDGE, MA 02139

OICY ATTN D.B. COX

OICY ATTN J.P. GILMORE

COMPUTER SCIENCES CORPORATION

6565 ARLINGTON BLVD

FALLS CHURCH, VA 22046

OICY ATTN H. BLANK

OICY ATTN JOHN SPOOR

OICY ATTN C. NAIL

COMSAT LABORATORIES

LINTHICUM ROAD

CLARKSBURG, MD 20734

OICY ATTN G. HYDE

ELECTROSPACE SYSTEMS, INC.

BOX 1359

RICHARDSON, TX 75080

OICY ATTN H. LOGSTON

OICY ATTN SECURITY (PAUL PHILLIPS)

ESL INCL.

495 JAVA DRIVE

SUNNYVALE, CA 94086

OICY ATTN J. ROBERTS

OICY ATTN JAMES MARSHALL

OICY ATTN C.W. PRETTIE

GENERAL ELECTRIC COMPANY

SPACE DIVISION

VALLEY FORGE SPACE CENTER

GODDARD BLVD KING OF PRUSSIA

P.O. BOX 8555

PHILADELPHIA, PA 19101

OICY ATTN M.H. BORTNER SPACE SCI LAB

GENERAL ELECTRIC COMPANY

P.O. BOX 1122

SYRACUSE, NY 13201

OICY ATTN F. REIBERT

GENERAL ELECTRIC COMPANY

TEMPO-CENTER FOR ADVANCED STUDIES

816 STATE STREET (P.O. DRAWER QQ)

SANTA BARBARA, CA 93102

OICY ATTN DASIAC

OICY ATTN DON CHANDLER

OICY ATTN TOM BARRETT

OICY ATTN TIM STEPHANS

OICY ATTN WARREN S. KNAPP

OICY ATTN WILLIAM MCNAMARA

OICY ATTN B. GAMBILL

OICY ATTN MACK STANTON

GENERAL ELECTRIC IECH SERVICES CO., INC.
HMES
COURT
SYRACUSE, NY 13201
O1CY ATTN G. MILLMAN

GENERAL RESEARCH CORPORATION
SANTA BARBARA DIVISION
P.O. BOX 6770
SANTA BARBARA, CA 93111
O1CY ATTN JOE ISE JR
O1CY ATTN JOEL GARBARINO

GEOPHYSICAL INSTITUTE
UNIVERSITY OF ALASKA
FAIRBANKS, AK 99701
(ALL CLASS ATTN: SECURITY OFFICERS)
O1CY ATTN T.N. DAVIS (UNCL ONLY)
O1CY ATTN NEAL BROWN (UNCL ONLY)
O1CY ATTN TECHNICAL LIBRARY
O1CY ATTN T. HALLINAN

ILLINOIS, UNIVERSITY OF
ATTN: DAN MCCLELLAN FOR K.C. YEH
150 DAVENPORT HOUSE
CHAMPAIGN, IL 61820

INSTITUTE FOR DEFENSE ANALYSES
400 ARMY-NAVY DRIVE
ARLINGTON, VA 22202
O1CY ATTN J.M. AEIN
O1CY ATTN HANS WOLFHARD
O1CY ATTN JOEL BENGSTON

HSS, INC.
2 ALFRED CIRCLE
BEDFORD, MA 01730
O1CY ATTN DONALD HANSEN

INTL TEL & TELEGRAPH CORPORATION
500 WASHINGTON AVENUE
NUTLEY, NJ 07110
O1CY ATTN TECHNICAL LIBRARY

JAYCOR
1401 CAMINO DEL MAR
DEL MAR, CA 92014
O1CY ATTN S.R. GOLDMAN

JOHNS HOPKINS UNIVERSITY
APPLIED PHYSICS LABORATORY
JOHNS HOPKINS ROAD
LAUREL, MD 20810
O1CY ATTN DOCUMENT LIBRARIAN
O1CY ATTN THOMAS PTEMRA
O1CY ATTN JOHN DASSOULAS

LOCKHEED MISSILES & SPACE CO INC
P.O. BOX 504
SUNNYVALE, CA 94088
O1CY ATTN DEPT 60-12
O1CY ATTN D.R. CHURCHILL

LOCKHEED MISSILES AND SPACE CO INC
3251 HANOVER STREET
PALO ALTO, CA 94304
O1CY ATTN MARTIN WALT DEPT 52-10
O1CY ATTN RICHARD G. JOHNSON DEPT 52-12
O1CY ATTN W.L. IMHOF DEPT 52-12
O1CY ATTN D. CAUFMAN

KAMAN SCIENCES CORP
P.O. BOX 7463
COLORADO SPRINGS, CO 80933
O1CY ATTN T. MEAGHER

LINKABIT CORP
10453 ROSELLE
SAN DIEGO, CA 92121
O1CY ATTN IRWIN JACOBS
O1CY ATTN I. ROTHMUELLER

LOWELL RSCH FOUNDATION, UNIVERSITY OF
450 AIKEN STREET
LOWELL, MA 01854
O1CY ATTN K. BIBL
O1CY ATTN B. REINISCH

M.I.T. LINCOLN LABORATORY
P.O. BOX 73
LEXINGTON, MA 02173
O1CY ATTN DAVID M. TOWLE
O1CY ATTN P. WALDRON
O1CY ATTN L. LOUGHLIN
O1CY ATTN D. CLARK
O1CY ATTN J. DAVIS

MARTIN MARIETTA CORP
ORLANDO DIVISION
P.O. BOX 5837
ORLANDO, FL 32805
O1CY ATTN R. HEFFNER

MCDONNELL DOUGLAS CORPORATION
5301 BOLSA AVENUE
HUNTINGTON BEACH, CA 92647
O1CY ATTN N. HARRIS
O1CY ATTN J. MOULE
O1CY ATTN GEORGE MROZ
O1CY ATTN W. OLSON
O1CY ATTN R.W. HALPRIN
O1CY ATTN TECHNICAL LIBRARY SERVICES

MISSION RESEARCH CORPORATION
735 STATE STREET
SANTA BARBARA, CA 93101
O1CY ATTN P. FISCHER
O1CY ATTN W.F. CREVIER
O1CY ATTN STEVEN L. GUTSCHE
O1CY ATTN D. SAPPENFIELD
O1CY ATTN R. BOGUSCH
O1CY ATTN RALPH KILB
O1CY ATTN R. HENDRICK
O1CY ATTN DAVE SOWLE
O1CY ATTN F. FAJEN
O1CY ATTN M. SCHEIBE
O1CY ATTN CONRAD L. LONGMIRE
O1CY ATTN WARREN A. SCHLUETER

MITRE CORPORATION, THE
P.O. BOX 208
BEDFORD, MA 01730
O1CY ATTN JOHN MORGANSTERN
O1CY ATTN G. HARDING
O1CY ATTN C.E. CALLAHAN

MITRE CORP
WESTGATE RESEARCH PARK
1820 DOLLY MADISON BLVD
MCLEAN, VA 22101
O1CY ATTN W. HALL
O1CY ATTN W. FOSTER

PACIFIC-SIERRA RESEARCH CORP
1456 CLOVERFIELD BLVD.
SANTA MONICA, CA 90404
O1CY ATTN E.C. FIELD JR

PENNSYLVANIA STATE UNIVERSITY
IONOSPHERE RESEARCH LAB
318 ELECTRICAL ENGINEERING EAST
UNIVERSITY PARK, PA 16802
(NO CLASSIFIED TO THIS ADDRESS)
O1CY ATTN IONOSPHERIC RESEARCH LAB

PHOTOMETRICS, INC.
442 MARRETT ROAD
LEXINGTON, MA 02173
O1CY ATTN IRVING L. KOFSKY

PHYSICAL DYNAMICS INC.
P.O. BOX 3027
BELLEVUE, WA 98009
O1CY ATTN E.J. FREMOUW

PHYSICAL DYNAMICS INC.
P.O. BOX 1069
BERKELEY, CA 94701
O1CY ATTN A. THOMPSON

R & D ASSOCIATES
P.O. BOX 9695
MARINA DEL REY, CA 90291
O1CY ATTN FORREST GILMORE
O1CY ATTN BRYAN GABBARD
O1CY ATTN WILLIAM B. WRIGHT JR.
O1CY ATTN WILLIAM J. KARZAS
O1CY ATTN ROBERT F. LELEVIER
O1CY ATTN H. ORY
O1CY ATTN C. MACDONALD
O1CY ATTN R. TURCO

RAND CORPORATION, THE
1700 MAIN STREET
SANTA MONICA, CA 90406
O1CY ATTN CULLEN CRAIN
O1CY ATTN ED BEDROZIAN

RIVERSIDE RESEARCH INSTITUTE
80 WEST END AVENUE
NEW YORK, NY 10023
O1CY ATTN VINCE TRAPANI

SCIENCE APPLICATION, INC.
P.O. BOX 2351
LAJOLLA, CA 92038
O1CY ATTN LEWIS M. LINSON
O1CY ATTN DANIEL A. HAMLIN
O1CY ATTN D. SACHS
O1CY ATTN E.A. STRAKER
O1CY ATTN CURTUS A. SMITH
O1CY ATTN JACK MCDUGALL

RAYTHEON CO.
528 BOSTON POST ROAD
SUDBURY, MA 01776
O1CY ATTN BARBARA ADAMS

SCIENCE APPLICATIONS, INC.
HUNTSVILLE DIVISION
2109 W. CLINTON AVENUE
SUITE 700
HUNTSVILLE, AL 35805
OICY ATTN DALE H. DAVIS

SCIENCE APPLICATIONS, INCORPORATED
8400 WESTPARK DRIVE
MCLEAN, VA 22101
OICY ATTN J. COCKAYNE

SCIENCE APPLICATIONS, INC.
80 MISSION DRIVE
PLEASANTON, CA 94566
OICY ATTN SZ

SRI INTERNATIONAL
333 RAVENSWOOD AVENUE
MENLO PARK, CA 94025
OICY ATTN DONARD NEILSON
OICY ATTN ALAN BURNS
OICY ATTN G. SMITH
OICY ATTN L.L. COBB
OICY DAVID A. JOHNSON
OICY ATTN WALTER G. CHESNUT
OICY ATTN CHARLES L. RINO
OICY ATTN WALTER JAYE
OICY ATTN M. BARON
OICY ATTN R. LIVINGSTON
OICY ATTN RAY L. LEADABRAND
OICY ATTN G. CARPENTER
OICY ATTN G. PRICE
OICY ATTN J. PETERSON
OICY ATTN R. HAKE, JR.
OICY ATTN V. GONZALES
OICY ATTN D. MCDANIEL
OICY ATTN R. TSUNODA

TECHNOLOGY INTERNATIONAL CORP
75 WIGGINS AVENUE
BEDFORD, MA 01730
OICY ATTN W.P. BOQUIST

UNIVERSITY OF TOKYO
ISAS
KOMABA, MEGURO-KU
TOKYO, JAPAN
OICY ATTN DR. K.I. OYAMA

MAX-PLANCK-INSTITUT
FUR PHYSIK UND ASTROPHYSIK
INSTITUT FUR EXTRATERRESTRICHE PHYSIK
8046 GARCHING B. MUNCHEN, GERMANY
OICY ATTN PROF. GERHARD HAERENDEL

TRW DEFENSE & SPACE SYS GROUP
ONE SPACE PARK
REDONDO BEACH, CA 90278
OICY ATTN R.K. PLEBUCH
OICY ATTN S. ALTSCHULER
OICY ATTN D. DEE

VISIODYNE, INC.
19 THIRD AVENUE
NORTH WEST INDUSTRIAL PARK
BURLINGTON, MA 01802
OICY ATTN CHARLES HUMPHREY
OICY ATTN J.W. CARPENTER

IONOSPHERIC MODELING DISTRIBUTION LIST
UNCLASSIFIED ONLY

PLEASE DISTRIBUTE ONE COPY (EXCEPT WHERE
NOTED OTHERWISE) TO EACH OF THE FOLLOWING
PEOPLE:

ADVANCED RESEARCH PROJECTS AGENCY (ARPA)
STRATEGIC TECHNOLOGY OFFICE
ARLINGTON, VA 22217

CAPT DONALD M. LEVINE

NAVAL RESEARCH LABORATORY
WASHINGTON, D.C. 20375

DR. R. MEIER - CODE 4141
DR. TIMOTHY COFFEY - CODE 4000
DR. S. OSSAKOW - CODE 4780
DR. J. GOODMAN - CODE 4180
DR. E. SZUSZCZEWICZ - CODE 4187 (50 COPIES)

DIRECTOR OF SPACE AND ENVIRONMENTAL LABORATORY
NOAA
BOULDER, CO 80302

DR. A. GLENN JEAN
DR. G. W. ADAMS
DR. D. N. ANDERSON
DR. K. DAVIES
DR. R. F. DONNELLY

AIR FORCE GEOPHYSICS LABORATORY
HANSKOM AIR FORCE BASE, MA 01731

DR. T. ELKINS
DR. W. SWIDER
MRS. R. SAGALYN
DR. J. M. FORBES
DR. T. J. KENESHEA
DR. J. AARONS
DR. R. NARCISI

OFFICE OF NAVAL RESEARCH
800 NORTH QUINCY STREET
ARLINGTON, VA 22217

U.S. ARMY ABERDEEN RESEARCH AND DEVELOPMENT
CENTER BALLISTIC RESEARCH LABORATORY
ABERDEEN, MD 21001

DR. J. HEIMERL

COMMANDER
NAVAL AIR SYSTEMS COMMAND
DEPARTMENT OF THE NAVY
WASHINGTON, D.C. 20360

DR. T. CZUBA

HARVARD UNIVERSITY
HARVARD SQUARE
CAMBRIDGE, MASS. 02138

DR. M. B. McELROY
DR. R. LINDZEN

PENNSYLVANIA STATE UNIVERSITY
UNIVERSITY PARK, PA 16802

DR. J. S. NISBET
DR. P. R. ROHRBAUGH
DR. D. E. BARAN
DR. L. A. CARPENTER
DR. M. LEE
DR. R. DIVANY
DR. P. BENNETT
DR. E. KLEVANS

UNIVERSITY OF CALIFORNIA, LOS ANGELES
405 HILLGARD AVENUE
LOS ANGELES, CA 90024

DR. R. STENZEL
DR. F. V. CORONITI
DR. C. KENNEL
DR. W. GEKELMAN

UNIVERSITY OF CALIFORNIA, BERKELEY
BERKELEY, CA 94720

DR. M. HUDSON

UTAH STATE UNIVERSITY
4TH AND 8TH STREETS
LOGAN, UTAH 84322

DR. P. M. BANKS
DR. R. HARRIS
DR. V. PETERSON
DR. R. MEGILL
DR. K. BAKER
DR. R. WILLIAMSON

CORNELL UNIVERSITY
ITHACA, N.Y. 14850

DR. W. E. SWARTZ
DR. R. SUDAN
DR. D. FARLEY
DR. M. KELLEY

NASA
GODDARD SPACE FLIGHT CENTER
GREENBELT, MD 20771

DR. S. J. BAUER/CODE 600
DR. R. HARTEL/CODE 621
DR. R. GOLDGERG/CODE 912
DR. S. CHANDRA
DR. K. MAEDO
DR. R. BENSON/CODE 621

PRINCETON UNIVERSITY
PLASMA PHYSICS LABORATORY
PRINCETON, N.J. 08540

DR. F. PERKINS
DR. E. FRIEMAN

INSTITUTE FOR DEFENSE ANALYSIS
400 ARMY/NAVY DRIVE
ARLINGTON, VA 22202

DR. E. BAUER

UNIVERSITY OF MARYLAND
COLLEGE PARK, MD 20742

DR. K. PAPADOPOULOS
DR. E. OTT

UNIVERSITY OF PITTSBURGH
PITTSBURGH, PA 15213

DR. N. ZABUSKY
DR. M. BIONDI

DEFENSE DOCUMENTATION CENTER
CAMERON STATION
ALEXANDRIA, VA 22314

(12 COPIES IF OPEN PUBLICATION
OTHERWISE 2 COPIES) 12 CY ATTN TC

UNIVERSITY OF CALIFORNIA
LOS ALAMOS SCIENTIFIC LABORATORY
J-10, MS-664
LOS ALAMOS, NEW MEXICO 87545

DR. M. PONGRATZ
DR. D. SIMONS
DR. G. BARASCH
DR. L. DUNCAN

OFFICE OF ASSISTANT SECRETARY OF NAVY
FOR RESEARCH, ENGINEERING AND SYSTEMS
PENTAGON RM 4D745
WASHINGTON, DC 20350

03 CY ATTN DR. H. RABIN
DEPUTY ASSISTANT
SEC. OF NAVY

SECURITY CLASSIFICATION OF THIS PAGE (When Data Entered)

REPORT DOCUMENTATION PAGE		READ INSTRUCTIONS BEFORE COMPLETING FORM
1. REPORT NUMBER NRL Memorandum Report 4531	2. GOVT ACCESSION NO.	3. RECIPIENT'S CATALOG NUMBER
4. TITLE (and Subtitle) THE STP/S3-4 SATELLITE EXPERIMENT: EQUATORIAL F-REGION IRREGULARITIES	5. TYPE OF REPORT & PERIOD COVERED Interim report on a continuing NRL problem.	
	6. PERFORMING ORG. REPORT NUMBER	
7. AUTHOR(s) M. Singh*, E. P. Szuszcwicz and J. C. Holmes	8. CONTRACT OR GRANT NUMBER(s)	
9. PERFORMING ORGANIZATION NAME AND ADDRESS Naval Research Laboratory Washington, DC 20375	10. PROGRAM ELEMENT, PROJECT, TASK AREA & WORK UNIT NUMBERS 61153N; RR033-02-44; 41-0949-0-1	
11. CONTROLLING OFFICE NAME AND ADDRESS Office of Naval Research Arlington, VA 22217	12. REPORT DATE July 14, 1981	
	13. NUMBER OF PAGES 16	
14. MONITORING AGENCY NAME & ADDRESS (if different from Controlling Office)	15. SECURITY CLASS. (of this report) UNCLASSIFIED	
	15a. DECLASSIFICATION/DOWNGRADING SCHEDULE	
16. DISTRIBUTION STATEMENT (of this Report) Approved for public release; distribution unlimited.		
17. DISTRIBUTION STATEMENT (of the abstract entered in Block 20, if different from Report)		
18. SUPPLEMENTARY NOTES *Present address: Sachs/Freeman Associates, Inc., Bowie, MD 20715 (On leave from Punjabi University, Patiala, India.)		
19. KEY WORDS (Continue on reverse side if necessary and identify by block number) Ionosphere Equatorial irregularities "In Situ" Satellite measurements		
20. ABSTRACT (Continue on reverse side if necessary and identify by block number) The S3-4 "in situ" satellite observations near the nighttime equator (2230 LT) have shown irregularity structures with depletions in plasma density up to 3 orders of magni- tude and ranges in horizontal extent from less than 1 km to tens of kms. The holes have sharper gradients on the eastern boundary than across the western counterpart, and the power spectral indices in the irregularities lie between 1.9-2.5 in the intermediate (Continues)		

DD FORM 1 JAN 73 1473

EDITION OF 1 NOV 65 IS OBSOLETE
S/N 0102-014-6601

SECURITY CLASSIFICATION OF THIS PAGE (When Data Entered)

20 ABSTRACT (Continued)

wavelength domain. The east-west asymmetry of the depletions is also shown in the irregularity intensity and spectral strengths. The variations in density are more intense on the western wall of the holes suggesting a scintillation enhancement on the western boundary. In addition, the results of power spectral analyses support the role of the Rayleigh-Taylor instability in the generation of intermediate scale size irregularities during the occurrence of equatorial spread-F.

CONTENTS

INTRODUCTION	1
EXPERIMENTAL RESULTS	2
Plasma Depletions	2
East-West Asymmetry	6
COMMENTS AND CONCLUSIONS	11
REFERENCES	12

THE STP/S3-4 SATELLITE EXPERIMENT: EQUATORIAL F-REGION IRREGULARITIES

INTRODUCTION

Equatorial F-region irregularities have drawn much interest in recent years because of their undesirable effects on trans-ionospheric communications and their cause-effect relationship with fundamental plasma instability processes. In efforts to understand the causative mechanism(s), considerable advances have been made in areas of detailed ground-based radar observations and "in situ" measurements. The radar observations (e.g., Woodman and La Hoz, 1976; Tsunoda et al. 1979) have found that meter-size irregularities primarily populate the bottomside F-region in the early evening, at later times tend to rise up and break away from their lower altitude source regime and develop structures extending up to the 700-1000 km region. These structures have come to be called "plumes".

On the macroscale (100's of meters to 10's of km) "in situ" nighttime equatorial measurements have revealed large biteouts in plasma density ranging up to three orders of magnitude (Hanson and Sanatani, 1973) and considered just as characteristic of spread-F as the much less intense (meter size) irregularities observed by radar. Later works on biteouts (Brinton et al. 1975; McClure et al. 1977) showed that ion composition inside and outside the holes can be vastly different. The molecular ions can be more abundant inside the holes than outside the holes, and the holes can vary from a few km to tens of km in the horizontal extent.

In examining potential relationships between radar plumes and ionospheric depletions, Szuszczewicz (1978) suggested that equatorial holes and spread-F were the same phenomena with small scale irregularities imbedded within the large scale depletions. He argued that a chemical volume of ion density on the bottomside (containing the signature of bottomside species) could move upward through a stationary neutral atmosphere and appear as biteouts at higher altitudes with much smaller structures (down to the meter range) populating the density gradients which bounded the macroscale depletion. This model was in concert with the numerical results of Scannapieco and Ossakow (1976) and the drift measurements of McClure et al. (1977).

To further study and definitively unfold the detailed relationships between large scale depletions, meter size irregularities and chemical transport processes, a coordinated investigation was conducted which involved simultaneous observations by radar and "in situ" rocket-borne diagnostics (Szuszczewicz et al., 1980). The combined observations have shown that

Manuscript submitted April 10, 1981.

(a) During conditions of well-developed equatorial spread-F the most intense "in situ" irregularities occurred on the bottom-side F-layer gradient.

(b) Within a large scale topside F-layer depletion radar backscatter and "in situ" irregularity strengths maximized near the depletion's upper wall.

(c) Ion composition within a topside depletion provided signatures of its bottomside source domain and estimates of average maximum vertical drift velocity. For long-lived depletions, it was found that molecular-ion signatures (NO^+ and O_2^+) can be lost while bottomside levels of N^+ can be maintained when $[\text{O}^+] \sim N_e \gg [\text{NO}^+] + [\text{O}_2^+]$; and finally,

(d) Large scale fluctuations of O^+ accompanied by a near-constant level of NO^+ and O_2^+ on the bottomside F-layer gradient suggests that neutral atmospheric turbulence was not a major source for bottomside ionospheric plasma irregularities and the associated triggering of equatorial spread-F.

To complement the vertical profile information provided by the rocket observations, we present and analyze a sample of "in situ" measurements conducted on the STP/S3-4 satellite carrying a pulsed plasma probe experiment. The probe experiment employed a self consistent test for measurement integrity, while determining electron density and temperature as well as density and mean ion mass fluctuations at 5-20 meter resolution. The S3-4 experiment has been discussed by Szuszczewicz et al. (1981). In this paper, we discuss some of the recent results with emphasis on general horizontal morphology, relationships to basic instability processes and associated scintillation effects.

EXPERIMENTAL RESULTS

Plasma Depletions

The data reported here was made available by the NRL-747 paired-pulsed-plasma-probes (P4) experiment (Szuszczewicz et al. 1981) on STP satellite S3-4 in a sun-synchronous orbit at lower F-region altitudes. The satellite crossed the nighttime equator at about 2230 LT when the frequency of occurrence of spread-F was high. One probe was biased to respond to variations in plasma electron saturation currents ($I_e \propto N_e$) and the other probe responded to the ion saturation

currents ($I_i \propto N_e / \sqrt{M_i}$). Subject to the selection of a number of commandable modes of operation, either probe could be repetitively pulsed from its fixed-bias level using a special electronic procedure (Holmes and Szuszczewicz, 1975) to generate conventional Langmuir characteristics for full determinations of electron density N_e , temperature T_e and plasma potential V_ϕ . The different modes of operation and experimental details are discussed by Szuszczewicz et al. (1981).

Figures 1 and 2 present samples of nighttime equatorial irregularity structures as measured by the currents collected by the electron (I_e) and ion (I_i) probes. The Figures show that the holes extend from a few kms to tens of kms, with depletion levels ranging from a factor of 3 (hole A) to a factor of 500 (hole F). A cursory analysis of Figures 1 and 2 reveals three particularly interesting observations:

(a) The density gradients on the opposing sides of each hole are different. Noting that the inclination of the satellite orbit is 96.4° (traveling in the east-to-west direction with time increasing left-to-right) it can be seen that density gradients in holes C-E (Fig. 1) and F (Fig. 2) are sharp on the eastern boundary and soft on each western counterpart. In the case of hole A, B and H (Fig. 1), the density gradients are not quite as sharp in comparison with holes C-F but the average density gradients are still softer on the western boundary. For the holes L (Fig. 1) and N' and L' (Fig. 2), the difference in density gradients on the opposing sides does not constitute any specific behavior while in the hole C' (Fig. 2) the density gradient is sharp on the western boundary. These observations can be summarized by noting that the density gradients are different across the boundaries of each depletion, with a preference for the density gradients to be sharper on the eastern side.

(b) Another interesting feature of the holes is their similarities in structural morphology. Holes A, B and H are similar in their horizontal profiles. A similarity feature can also be identified in the depletion L (Figure 1) and L' (Figure 2). Both of these depletions have a center point (M and M' respectively) around which the structures look similar. At the central point (M and M'), the plasma density approaches the background (undisturbed) level suggesting that one large hole is breaking up or alternatively two smaller ones are merging.

(c) The top panel of Figures 1 and 2 displays relative density fluctuations, $\delta I/I$ determined by variations about

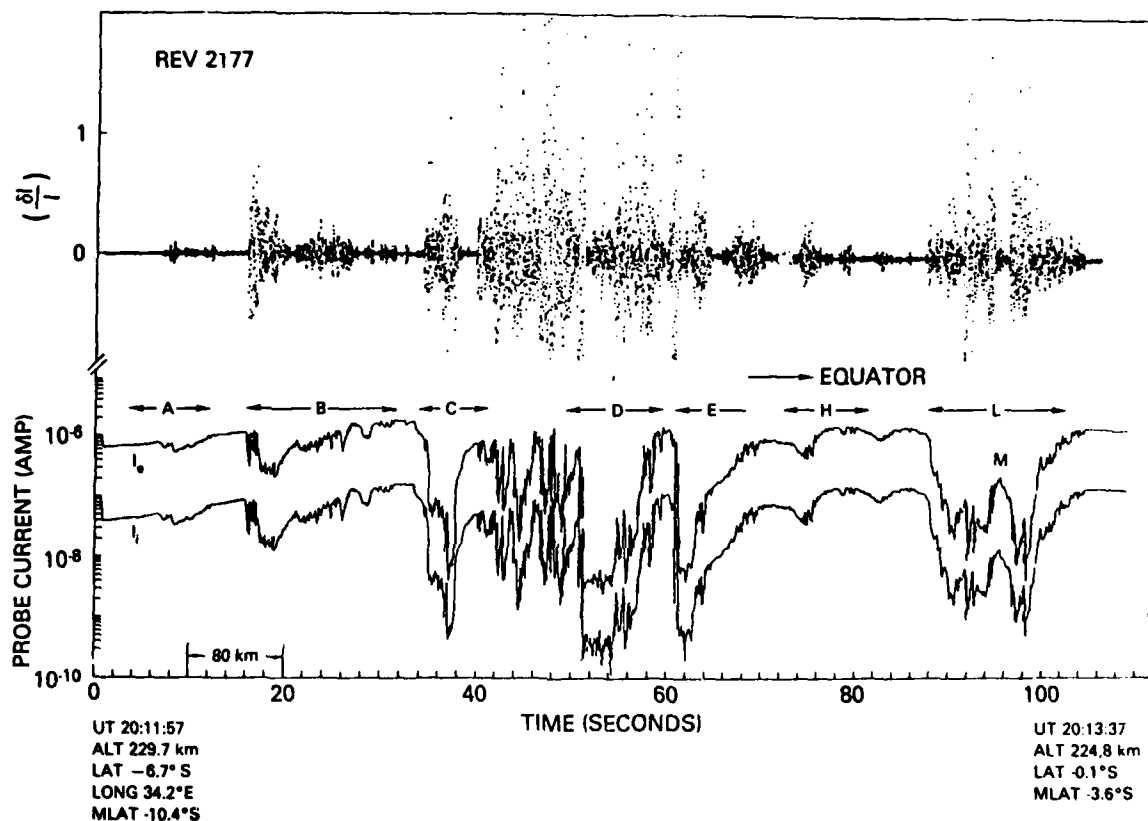


Figure 1

Horizontal profile of ionospheric F-region plasma density as indicated by electron (I_e) and ion (I_i) saturation currents measured on rev^e#2177. $\delta I/I$ is the relative irregularity intensity as calculated by variations about linear detrends over sliding 2.1 km intervals.

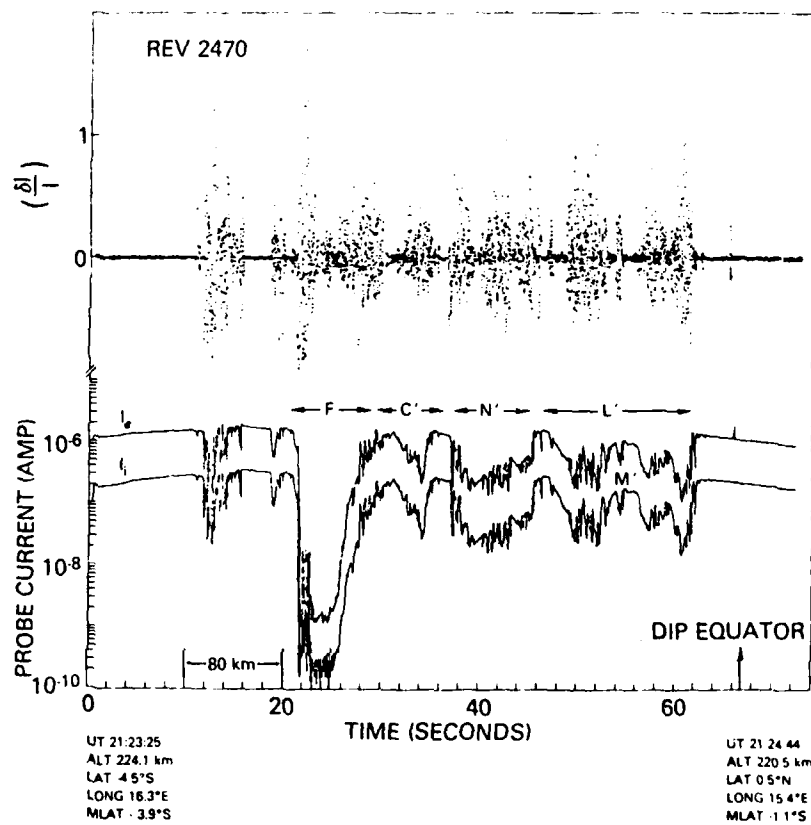


Figure 2

Horizontal profile of ionospheric F-region plasma density as indicated by electron (I_e) and ion (I_i) saturation currents measured on rev^e#2470. $\delta I/I_i$ is the relative irregularity intensity as calculated by variations about linear detrends over sliding 2.1 km intervals.

linear detrends over sliding 2.1 km intervals throughout the depletions. The fluctuations ($\delta I/I$) easily identifies the degree of disturbance. The percent variation in the holes A, B and H (Figure 1) is less than 20% in most parts, while in other holes of Figures 1 and 2 the variation can be more than 50%. In addition, the variations can be different across the opposing boundaries of the holes. We discuss this more fully below.

East-West Asymmetry

Further illustrations of F-region irregularities appear in data revs 2122 and 2123 shown in Figure 3. Rev 2123 shows four depletions (numbered 1 through 4) with the depletion level extending to more than two orders of magnitude. The rev 2122 shows three depletions (numbered 5 through 7) with depletions in density up to one order of magnitude.

The discussion is facilitated by identifying certain features in rev 2123. First, there are clearly defined regions of undisturbed background ionosphere, marked alphabetically A through D; the smoothness of the relative density and the corresponding 0% fluctuations attest to their undisturbed nature. Focussing on depletions 3 and 4, we see that the irregularity intensities are 2 to 3 times larger on the western boundary than on eastern counterparts. This same relationship is true in depletions 1 and 2, but only after a qualification that suggests that 1 and 2 are halves of a larger depletion bounded by A and B. This is supported in part by the non-existence of a quiescent ionosphere between the two. When viewed from this perspective the western boundary is approximately twice as intense in irregularity intensity as the eastern boundary. In rev 2122, the depletions 6 and 7 show the irregular intensity as more intense on the western boundary by a factor of 3-4. (On the basis of similar considerations applied to Figures 1 and 2, we note that the irregularity intensity is greater on the western boundaries of depletions D, E and H (Figure 1) and F (Figure 2), while the eastern boundary in holes A-C (Figure 1) is more intense. Based on irregularity intensity ($\delta I/I$) observations, we conclude that there is a high probability of occurrence of more intense fluctuations across the western boundary of bottomside F-region depletions.

The asymmetry in irregularity strengths and relationships to plasma instability mechanisms can be explored further through power spectral density analyses. We present in Figures 4 and 5 just such results for each of the boundaries in Figure 3 (1E and 1W refer respectively to the eastern and western boundary of depletion number 1). Though the experiment

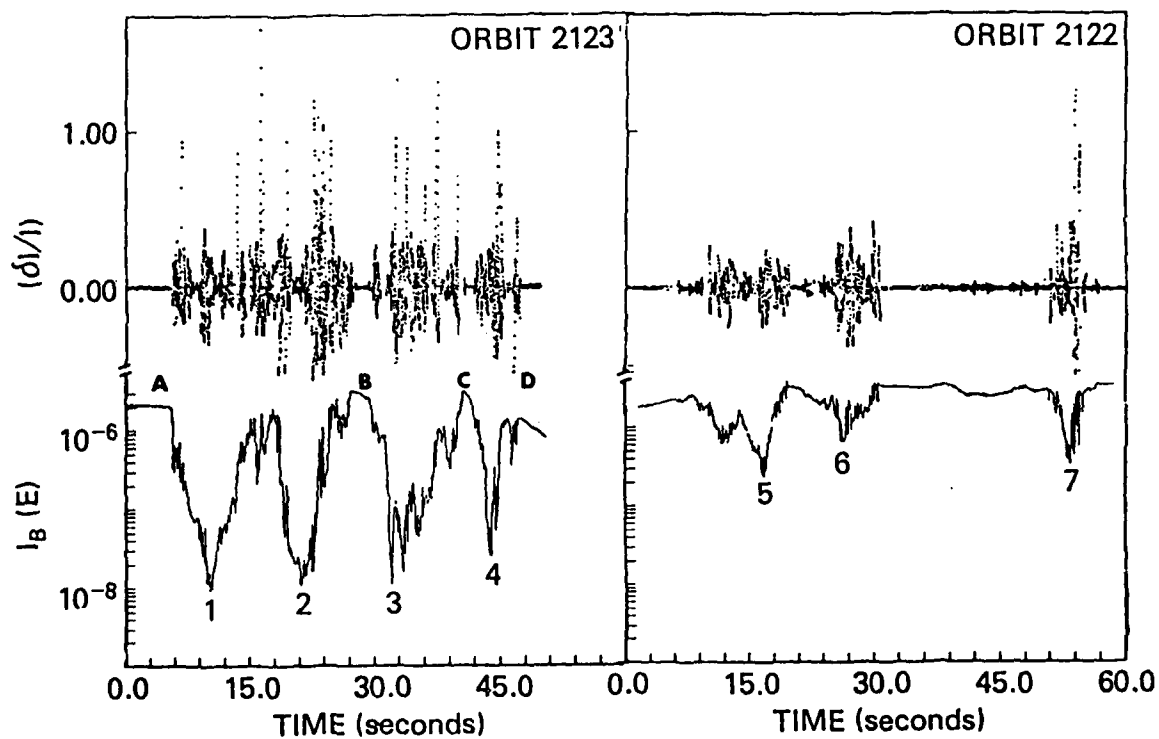


Figure 3

The electron density variation (as indicated by $I_B(E)$) for rev #2122 and 2123 along with irregularity intensity ($\delta I/I$) determined over contiguous 2.1 km intervals throughout the depletion.

provides the density fluctuation power spectra with a maximum Nyquist frequency of 400 Hz (19 m resolution along the orbit and 3-5 m resolution perpendicular to magnetic field) the data in this figure has been decimated by a factor of 3 in order to include greater spatial domains across the depletion walls. Power spectral analyses are presented across the boundaries of each of the seven depletions with spectral indices (n , in the equation $P = P_0 f^{-n}$) ranging from 1.9 to 2.5. More important however, is the ratio of spectral strengths (entered as $P_1 \equiv P_0(\text{west})/P_0(\text{east})$ in Figures 4 and 5) found to be 1.4 to 11.3 times more intense on the western boundaries. These intensity ratios extend down to a 15 meter wavelength perpendicular to the geomagnetic field. The spectral indices support the work of Keskinen et al. (1980) which predicts the same approximate range of values for horizontal irregularity structures perpendicular to \vec{B} . The east-west asymmetry in the depletions is apparent from the linear detrend of data and the ratio of spectral strengths.

We now show that the asymmetry bears on scintillation observations. To do this we note that scintillations depend upon ΔN ($\Delta N \propto \Delta I$) rather than $\Delta N/N$ (as calculated by

$\frac{\Delta I}{I}$) and the power spectral analysis $P_0 \propto \left(\frac{\Delta I}{I}\right)^2$. For the purpose of scintillation-effect calculations, we have determined

$|\Delta I|_{\text{r.m.s.}}$ in the wavelength domain 80 m to 8 km by assuming that $P_{\text{r.m.s.}}$ in this domain is equal to $(|\Delta I|_{\text{r.m.s.}}/I)^2$.

Defining P_2 as

$$P_2 = \frac{(\Delta I)_{\text{r.m.s.}} (\text{in the wavelength range 80m-8km on the west wall})}{(\Delta I)_{\text{r.m.s.}} (\text{in the wavelength range 80m-8km on the east wall})}$$

we find the values of P_2 ranging from 1.1 to 7.7. These results suggest enhanced scintillation effects on the western wall of the depletions, in agreement with the observations of Livingston et al. (1980). Furthermore, the radar measurements (Tsunoda, 1979) also show that the bottomside backscatter strength is often asymmetric in the east-west plane with stronger backscatter from the western wall of a plume. The combined observations support a model of E-W asymmetry which allows for a neutral-wind driven instability growth rate enhancement on the western side of a rising bottomside F-region depletion. The maximum growth rate occurs on the western wall of the rising depletion, where the electron density gradient is most closely aligned with the plasma drift velocity vector in the reference frame of the neutral wind (Tsunoda, 1979; Zalesak et al. 1980).

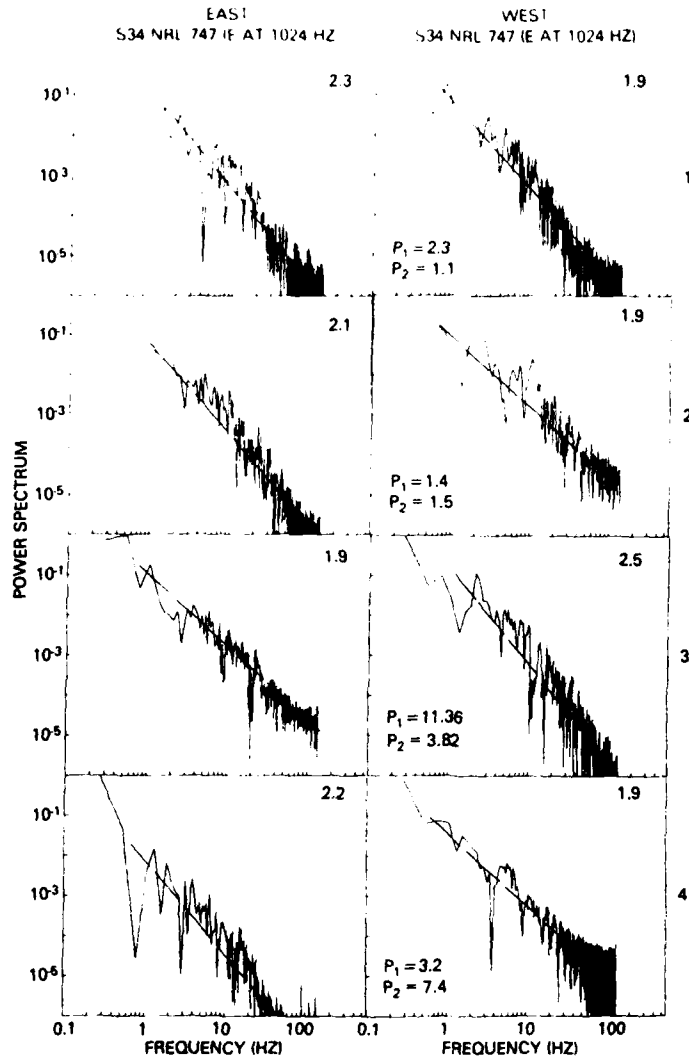


Figure 4

Power spectral analyses across the boundaries of the four depletions (1 through 4) of rev #2123 in Figure 3. The number in the upper right portion of each panel is the spectral index (n in the equation

$P = P_0 k^{-n}$). The value P_1 in each right panel is the ratio of spectral strengths (P_0) of western to eastern boundary $P_1 = P_0(\text{West})/P_0(\text{East})$. The value P_2 is the ratio of r.m.s. value of spectral strength in the wavelength domain (80 m-8 Km) of western to eastern boundary ($P_2 = P_{\text{r.m.s.}}(\text{West})/P_{\text{r.m.s.}}(\text{East})$).

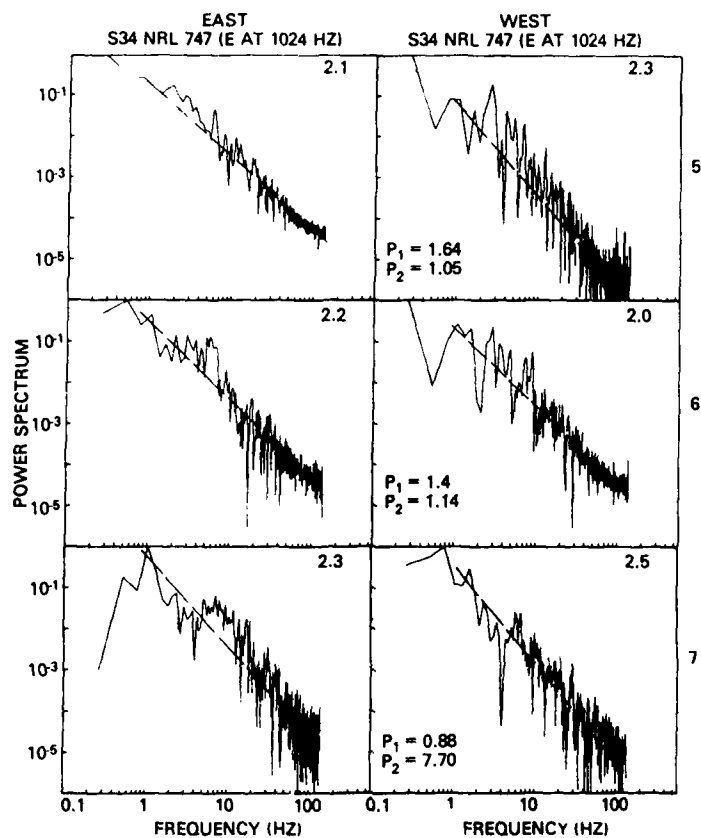


Figure 5

Power spectral analyses across the boundaries of the four depletions (5 through 7) of rev #2122 in Figure 3. The number in the upper right portion of each panel is the spectral index (n in the equation

$P = P_0 k^{-n}$). The value P_1 in each right panel is the ratio of spectral strengths (P_0) of western to eastern boundary $P_1 = P_0(\text{West})/P_0(\text{East})$. The value P_2 is the ratio of r.m.s. value of spectral strength in the wavelength domain (80 m-8 Km) of western to eastern boundary ($P_2 = P_{\text{r.m.s.}}(\text{West})/P_{\text{r.m.s.}}(\text{East})$).

COMMENTS AND CONCLUSIONS

The results of the high resolution S3-4 satellite experiment for equatorial F-region irregularities show large scale plasma depletions (1 km to 10's of km wide) with smaller scale irregularities superimposed (smallest detectable scale size ~ 10 meters perpendicular to \vec{B}). The depletions (which may in fact represent the bottomside upwelling process that has come to be identified with the lower F-region manifestations of spread-F) show east-west asymmetry with the irregularity intensity and spectral strengths generally more intense on the western boundary. Associated calculations over density fluctuations in the range 80 meters to 8 km suggest that scintillation effects would be similarly more intense on the western boundary. We find these observations consistent with radar (Tsunoda, 1979) and scintillation measurements (Livingston et al. 1980) as well as the recent computational work of Zalesak et al. (1980). Furthermore, we find the horizontal power spectral indices to lie between 1.9-2.5, supporting the role of Rayleigh-Taylor instability (Keskinen et al. 1980) and the recent theoretical and experimental comparison in the vertical plane (Keskinen et al. 1981).

REFERENCES

- Brinton, H.C. H.G. Mayr, and G.P. Newton, "Ion composition in the nighttime equatorial F-region: Implications for chemistry and dynamics", (abstract) EOS Trans. AGU 56 1038 (1975).
- Hanson, W.B. and S. Sanatani, "Large N₁ gradients below equatorial F-peak", J. Geophys. Res. 78, 1167 (1973).
- Holmes, J.C. and E.P. Szuszcwicz, "A versatile plasma probe", Rev. Sci. Instr. 46, 592 (1975).
- Keskinen, M.J., S.L. Ossakow and P.K. Chaturvedi, "Preliminary report on numerical simulations of intermediate wavelength collisional Rayleigh-Taylor instability in equatorial spread-F", J. Geophys. Res. 85, 1775 (1980).
- Keskinen, M.J., E.P. Szuszcwicz, S.L. Ossakow and J.C. Holmes, "Nonlinear theory and experimental observations of the local collisional Rayleigh-Taylor instability", J. Geophys. Res. (1981, in press).
- Livingston, R.C., E. Weber and T. Bauchau, "Multi-scale observations of irregularities in an isolated and decaying plasma bubble", Paper presented at International Symposium on Equatorial Aeronomy, Aguidilla, P.R., July 1980.
- McClure, J.P., W.B. Hanson and J.N. Hoffman, "Plasma bubbles and irregularities in the equatorial ionosphere", J. Geophys. Res. 82, 2650 (1977).
- Scannapieco, A.J. and S.L. Ossakow, "Non linear equatorial spread-F", Geophys. Res. Lett. 3, 451 (1976).
- Szuszcwicz, E.P., "Ionospheric holes and equatorial spread-F: Chemistry and transport", J. Geophys. Res. 83, 2665 (1978).
- Szuszcwicz, E.P., R.T. Tsunoda, R. Narcisi, and J.C. Holmes, "Coincident radar and rocket observations of equatorial spread-F", Geophys. Res. Lett. 7, 537 (1980).
- Szuszcwicz, E.P., J.C. Holmes and M. Singh, "The STP/S3-4 ionospheric irregularity satellite experiment", J. Geophys. Res. (1981, submitted).
- Tsunoda, R.T., "The growth and decay of equatorial backscatter plumes", DNA report, SRI International, (Nov. 1979).

Tsunoda, R.T., M.J. Baron, J. Owen and D.M. Towle, "Altair: An incoherent scatter radar for equatorial spread-F studies", Radio Sci. 14, (1979).

Woodman, R.F. and C. La Hoz, "Radar observations of F-region equatorial irregularities", J. Geophys. Res. 81, 5447 (1976).

Zalesak, S.T., S.L. Ossakow and P.K. Chaturvedi, "An explanation of westward tilts, fishtails and C's in the equatorial spread-F ionosphere", EOS Trans. AGU 61, 1059 (1980).

REPORT DOCUMENTATION PAGE		READ INSTRUCTIONS BEFORE COMPLETING FORM
1. REPORT NUMBER	2. GOVT ACCESSION NO.	3. RECIPIENT'S CATALOG NUMBER
NRL Memorandum Report 4728		
4. TITLE (and Subtitle)		5. TYPE OF REPORT & PERIOD COVERED
THE S3-4 IONOSPHERIC IRREGULARITIES SATELLITE EXPERIMENT: PROBE DETECTION OF MULTI-ION COMPO- NENT PLASMAS AND ASSOCIATED EFFECTS ON INSTA- BILITY PROCESSES		Interim report on a continuing NRL problem.
7. AUTHOR(s)		6. PERFORMING ORG. REPORT NUMBER
E. P. Szuszcwicz, J. C. Holmes, and M Singh*		
9. PERFORMING ORGANIZATION NAME AND ADDRESS		8. CONTRACT OR GRANT NUMBER(s)
Naval Research Laboratory Washington, DC 20375		
11. CONTROLLING OFFICE NAME AND ADDRESS		10. PROGRAM ELEMENT, PROJECT, TASK AREA & WORK UNIT NUMBERS
Office of Naval Research Arlington, VA 22217		61153N; RR033-02-44; 41-0949-0-2
14. MONITORING AGENCY NAME & ADDRESS (if different from Controlling Office)		12. REPORT DATE
		February 11, 1982
		13. NUMBER OF PAGES
		30
		15. SECURITY CLASS. (of this report)
		UNCLASSIFIED
		15a. DECLASSIFICATION/DOWNGRADING SCHEDULE
16. DISTRIBUTION STATEMENT (of this Report)		
Approved for public release; distribution unlimited.		
17. DISTRIBUTION STATEMENT (of the abstract entered in Block 20, if different from Report)		
18. SUPPLEMENTARY NOTES		
*Present address: Sachs/Freeman Associates, Inc., Bowie, MD 20715. On leave from Punjabi University, Patiala, India.		
19. KEY WORDS (Continue on reverse side if necessary and identify by block number)		
Ionospheric irregularities Power spectrum Satellite measurements Plasma diagnostics		
20. ABSTRACT (Continue on reverse side if necessary and identify by block number)		
<p>The pulsed plasma probe technique has been expanded to include simultaneous determinations of absolute electron density, density fluctuations, electron temperature, and mean ion mass with resolution limited only by probe geometry, sheath size, and telemetry. The technique has been designed to test for coupling of electron density variations and ion composition irregularities in multi-component plasmas by the comparison of electron density fluctuation power spectra $P_N(k)$ and a newly developed diagnostic parameter, the mean ion mass fluctuation spectra $\delta \bar{M}_i / \bar{M}_i \rightarrow P_M(k)$. In addition, the experiment</p> <p style="text-align: right;">(Continues)</p>		

20 ABSTRACT (Continued)

extends satellite-borne irregularity spectral analyses down to the 5-20 meter range while attempting to synthesize F-region plasma instability processes on the basis of N_e , T_e , ΔN_e , P_N and P_M . Initial results demonstrate the expanded diagnostic capability for high spatial resolution measurements of mean ion mass and provide experimental evidence for the role of ion composition in multi-stepped plasma instability processes. Specific results include a spectral index X_n in $P_N = A_n f^{-X_n}$ of 1.6-2.9 over the wavelength range from 1 km to 6 meters under conditions identified with an unstable equatorial nighttime ionosphere. Simultaneous measurements of $\delta \bar{M}_i / \bar{M}_i \rightarrow (P_M = A_m f^{-X_m})$ and $\delta N_e / \bar{N}_e \rightarrow (P_N = A_n f^{-X_n})$ have shown a general behavior tending to lower power ($A_m < A_n$) and softer spectra ($X_m < X_n$) in ion mass fluctuations when compared with fluctuations in total plasma density. Limited analyses of the two power spectral elements raises hopes for the differentiation between plasma mechanisms that can lead to similar indices in P_N .

CONTENTS

INTRODUCTION	1
THE EXPERIMENTAL TECHNIQUE	6
DATA ANALYSIS AND RESULTS	11
COMMENTS AND CONCLUSIONS	23
ACKNOWLEDGMENT	24
REFERENCES	25

**THE S3-4 IONOSPHERIC IRREGULARITIES SATELLITE EXPERIMENT:
PROBE DETECTION OF MULTI-ION COMPONENT PLASMAS
AND ASSOCIATED EFFECTS ON INSTABILITY PROCESSES**

INTRODUCTION

In recent years interest in ionospheric research has turned from the definition of the zero-order ionosphere to an understanding of the more dynamic processes involving plasma instability mechanisms and their cause-effect relationships. While much progress has been made, more detailed experimental and theoretical work is needed to unfold the active first principles that govern the geoplasma environment. For example, we have yet to define the electron density fluctuation power spectrum over the broad domain encompassed by equatorial spread-F (tens of kilometers to fractions of a meter).

It is noted that density fluctuation power spectra represent an important approach to understanding the multi-stepped plasma processes in which large scale irregularities cascade to much smaller dimensions. In this regard the works of Dyson et al. (1974), along with the cataloging efforts of McClure and Hanson (1973) have identified some characteristic spectral features down to 70 meters. From here the definition of spectral characteristics needs to be extended down to sizes less than 1 meter (e.g., Huba et al. 1978 and associated references), and the same spectral characteristics must be studied within the context of positions relative to the F-layer peak (Ossakow et al, 1979) and any superimposed ionospheric depletions (McClure et al. 1977 and Szuszcwicz, 1978). These measurements must be time correlated in order to study the development of multi-step instability processes.

Extended studies of fluctuation power spectra cannot stand alone in determining all the causal mechanisms. Existing equatorial data show that studies of F-region irregularities must determine the degree of balance between the chemistry and dynamics. To this end, the temperature and high resolution ion composition measurements must be made inside and outside of ionospheric holes, as well as across the sharp boundaries that are a characteristic feature of many of the depleted domains. The temperature measurement should also be done simultaneously with the determination of electron density power spectra in order to determine the role of electron energy in the naturally occurring instability processes (Ossakow, 1974).

In order to develop a more comprehensive experimental profile on ionospheric irregularity structures, the pulsed plasma probe technique (Szuszczewicz and Holmes, 1975) has been expanded to include measurements of electron density fluctuations and variations in mean ion mass. These measurements are conducted simultaneously with the standard determinations of absolute electron density (N_e), temperature (T_e) and plasma potential (V_∞). The capability for high spatial resolution measurements of mean ion mass opens up the possibility of exploring the coupling of electron density variations and ion composition irregularities by the comparison of electron density fluctuation power spectra $P_N(k)$ and a newly developed

parameter, the mean ion mass fluctuation power spectra, $P_M(k)$. The new instrument (designated NRL-747) has been successfully flown on the lower F-region, polar orbiting, sun-synchronous (2230 LT equatorial crossing) STP/S3-4 satellite launched in March 1978. The orbit allows a global study of N_e , T_e and $P_N(k)$, an information set that will help catalogue similarities and differences between polar and equatorial irregularities and ultimately sort out first and second-order cause-effect relationships operating between plasma instabilities and ionospheric irregularities. The experiment provides the first effort to study the role of ion composition in the distribution of wave energy in the cascading process of large-to-small scale ionospheric plasma irregularities, a role considered important at the equator during the occurrence of spread-F conditions and potentially important at high latitudes under conditions of current-convective instability.

Figure 1 schematically depicts the latitudinal differences in the irregular ionosphere at F-region altitudes, with one of the initial investigative targets in the S3-4 effort being the complete experimental definition of thermal electron distributions in the "biteouts" at nighttime equatorial latitudes under spread-F conditions. These "biteouts" are naturally occurring ionospheric holes which can be three decades deep in depletion and can have widths ranging from fractions of a kilometer to tens of kilometers (see e.g., McClure et al., 1973 and 1977; Szuszczewicz, 1978; and

Szuszczeicz et al., 1981). There can be major changes in ion chemistry which take place across the boundaries of the holes...changes which now appear to be trendable and strongly coupled to the mechanism(s) which generate the holes themselves (Szuszczeicz et al., 1980; Narcisi and Szuszczeicz, 1981), and cascade the irregularity distributions from 10's of kilometers to fractions of a meter (e.g., Keskinen et al., 1981; Kelly et al., 1981).

Outside the latitudinal domain of equatorial spread-F, the regions of primary interest in the S3-4 study of F-region irregularities involve the main trough, auroral oval, and domains encompassing the ring current, polar wind and the cusp. The mid-latitude and dayside equatorial F-regions are generally very regular in structure and consequently of less interest.

Within the framework of the relatively simple picture in Figure 1, the improved plasma diagnostic capabilities on the S3-4 satellite and associated analysis efforts will attempt to assemble a relatively comprehensive catalogue of polar and equatorial irregularities along with an improved understanding of their cause-effect relationships. Indeed, some initial efforts have already been published (Singh et al., 1981; Rodriguez et. al., 1981; and Szuszczeicz et al., 1981). In the subsequent sections, the experimental technique will be described, associated data presented, and evidence will be provided which suggests that ion composition plays an important role in multi-stepped plasma instability processes active in the F-region ionosphere.

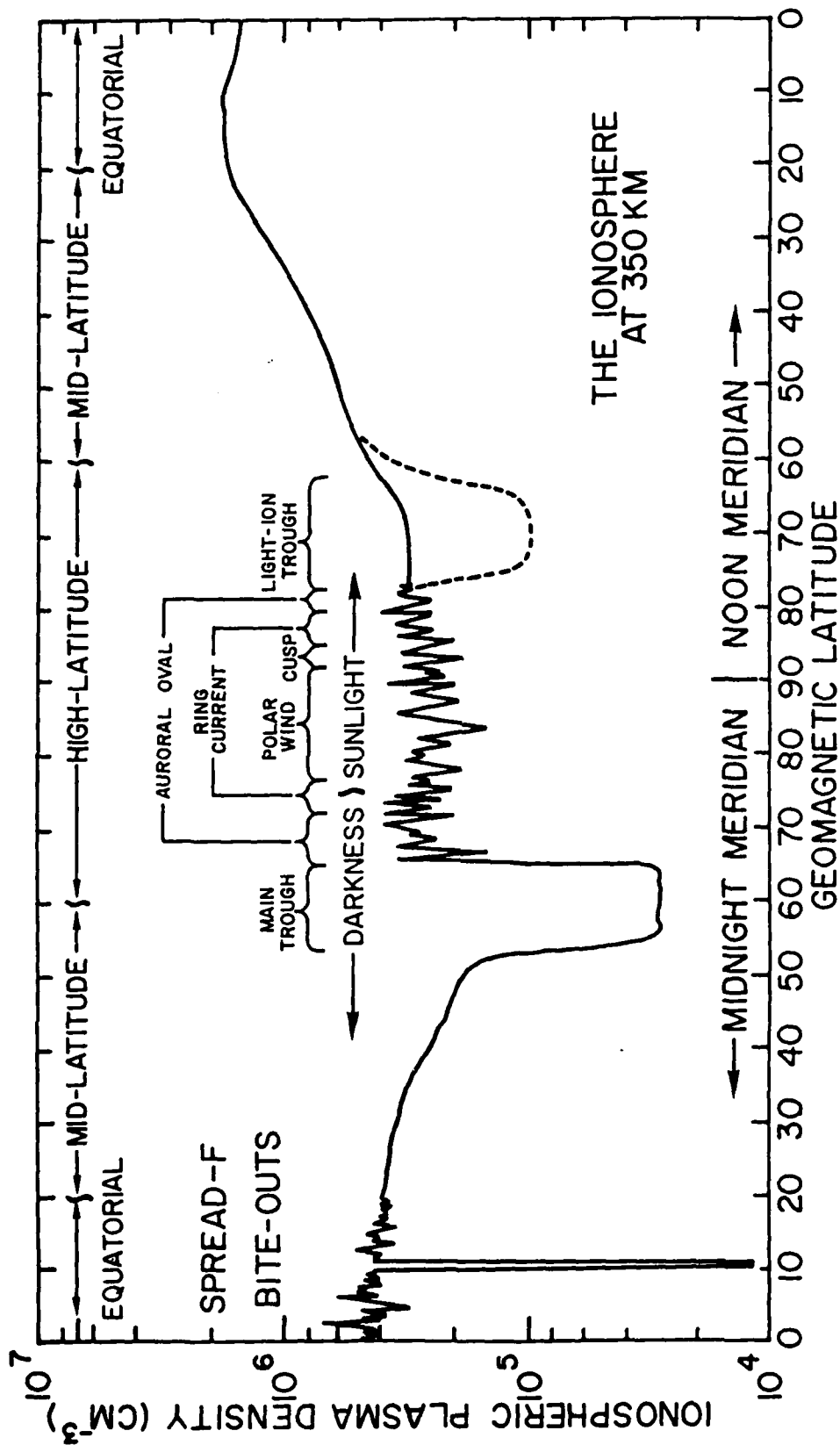


Fig. 1 — Schematic representation of F-region plasma density irregularities and associated geophysical domains

THE EXPERIMENTAL TECHNIQUE

The NRL-747 experiment employs a pair of pulsed plasma probes (P^4 is the designated acronym), each of which is capable of simultaneous measurement of electron density, temperature and density fluctuation power spectra regardless of the state of turbulence or the degree of irregularity in the ionospheric plasma medium. Together, the pair of probes also provide mean ion mass fluctuation measurements to a maximum Nyquist frequency of 200 Hz. The instrument is a Langmuir-type probe using a special electronic procedure for generating the current-voltage characteristic (Holmes and Szuszczewicz, 1975; Szuszczewicz and Holmes, 1975). The pulse modulated approach reduces the distortion of the current-voltage characteristic that can result from surface contamination and allows millisecond tracking of density fluctuations that might occur during the time required to generate the current voltage characteristic. (The temporal resolution is limited only by telemetry.)

Subject to the selection of 1 of 8 commandable modes of operation, each of the probes had applied to it some variation of the voltage function illustrated in Figure 2. The pulse modulated waveform, following the sawtooth envelope, provides the fundamental data set for a "conventional" Langmuir current-voltage characteristic and associated determinations of N_e and T_e (Chen, 1965) at a nominal 3 Hz rate. During the interpulse period, a fixed-voltage V_B is applied, with

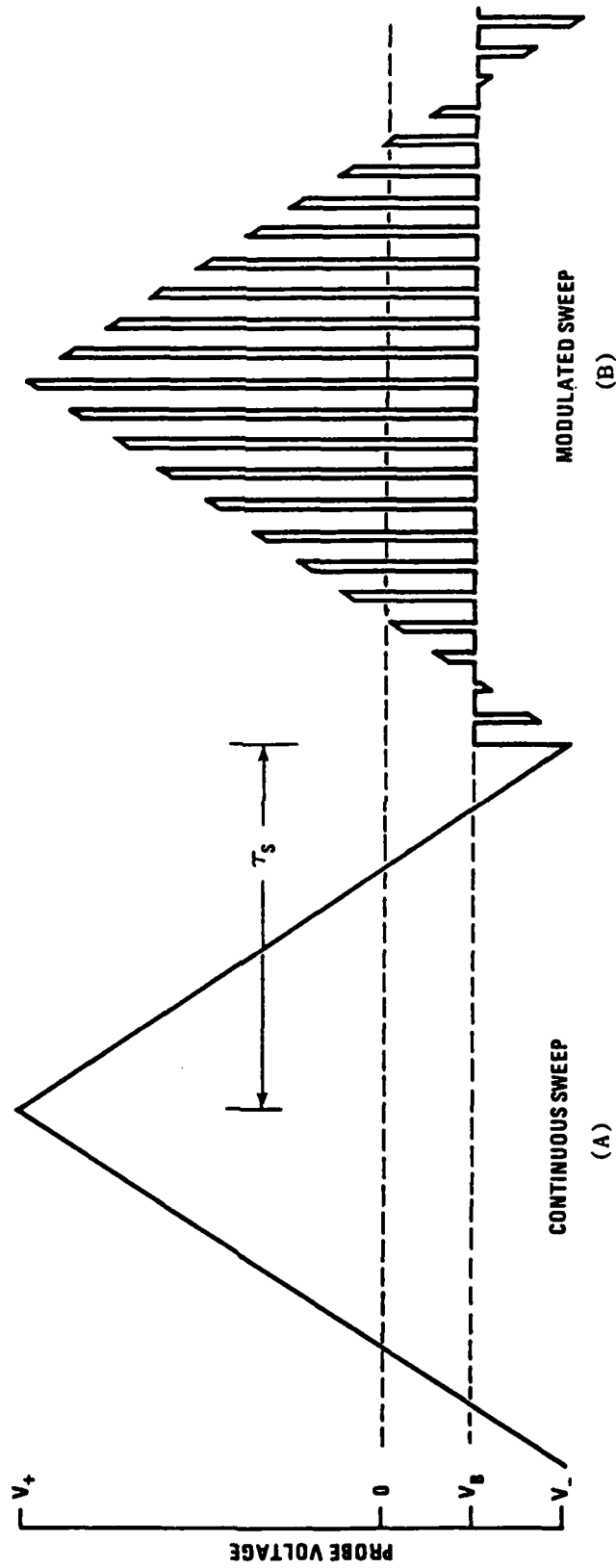


Fig. 2 — Voltage format utilized in the pulsed-sweep mode of the pulsed-plasma-probe (P^3) technique

associated current measurements providing a running measure of density fluctuations (assuming $\delta I_B \propto \delta N_e$) and a time-dependent data set for power spectral analysis with a Nyquist frequency of 400 Hz in the high data-rate mode. In addition to pulse-modulation, each of the probes could be operated in a simple fixed-bias mode and as a "conventional" continuous-sweep Langmuir probe, the latter having been introduced for systematic studies of hysteresis and contamination effects during satellite mission lifetimes (a minor mission objective).

The probes were routinely operated with V_B on one probe set for electron-saturation-current collection (defined as the E-probe with $I_B = I_e(\text{sat}) \equiv E$) while the value of V_B on the second probe was biased for ion saturation current collection (defined as the I probe with $I_B = I_i(\text{sat}) \equiv I$). The expressions for the currents collected by the two cylindrical probes take the forms

$$E \equiv I_e(\text{sat}) = N_e \sqrt{\frac{kT_e}{2\pi M_e}} A_p e \left\{ \sqrt{\frac{2}{\pi}} \left(1 + \frac{e\phi_p^e}{kT_e} \right)^{\frac{1}{2}} \right\} \quad (1)$$

(Chen, 1965; for thick sheaths) and

$$I \equiv I_i(\text{sat}) = N_i \sqrt{\frac{kT_i}{2\pi M_i}} A_p e \left\{ \sqrt{\frac{2}{\pi}} \left(\frac{|e\phi_p^i|}{kT_i} + \frac{M_i w^2}{2kT_i} \right)^{\frac{1}{2}} \right\} \quad (2)$$

(Hoegy and Wharton, 1973; for probe axis perpendicular to the vehicle velocity vector in the ionospheric plasma rest frame). In the above equations A_p is the probe area, $M_{e(i)}$ and $N_{e(i)}$ are the mass and density of the electron (ion)

population, $T_{e(i)}$ is the associated temperature of an assumed Maxwellian distribution, e is the fundamental electron charge, k is Boltzmann's constant, w is the satellite velocity and $\phi_p^{e(i)}$ is the baseline voltage V_B applied to the E (I) probe and referenced to the plasma potential ($\phi_p^{e(i)} = V_B - V_\infty$).

The square of the ratio $I_e(\text{sat})/I_i(\text{sat})$ can be written

$$\left(\frac{I_e(\text{sat})}{I_i(\text{sat})} \right)^2 \equiv \left(\frac{E}{I} \right)^2 = \frac{T_e}{T_i} \frac{M_i}{M_e} \left\{ \frac{1 + |e\phi_p^e/kT_e|}{(M_i w^2/2kT_i + |e\phi_p^i/kT_i|)} \right\} \quad (3)$$

with additional manipulation (assuming $|e\phi_p^e| \gg kT_e$) resulting in

$$\left(\frac{I_e(\text{sat})}{I_i(\text{sat})} \right)^2 = \frac{M_i}{M_e} \left| \frac{\phi_p^e}{\phi_p^i} \right| \quad \frac{1}{2} M_i w^2 \ll e\phi_p^i \quad (4a)$$

$$\left(\frac{I_e(\text{sat})}{I_i(\text{sat})} \right)^2 = \frac{2 |e\phi_p^e|}{M_e w^2} \quad \frac{1}{2} M_i w^2 \gg e\phi_p^i \quad (4b)$$

$$\left(\frac{I_e(\text{sat})}{I_i(\text{sat})} \right)^2 = \frac{M_i}{M_e} \left| \frac{\phi_p^e}{\phi_p^i} \right| \left(1 + \frac{M_i w^2}{2e\phi_p^i} \right)^{-1} \quad \frac{1}{2} M_i w^2 \approx e\phi_p^i \quad (4c)$$

For laboratory and rocket-borne experiments equation (4a) would apply, whereas in the S3-4 satellite investigation equation (4c) applies. Equation (4c) is plotted in Figure 3 for two sets of bias potentials, $(|\phi_p^e|, |\phi_p^i|) = (2V, 1V)$ and $(1V, 2V)$. The results in Figure 3 show that with limitations placed on the ratio ϕ_p^e/ϕ_p^i , variations in $(I_e/I_i)^2$ can be taken as a direct measure of ion mass variations.

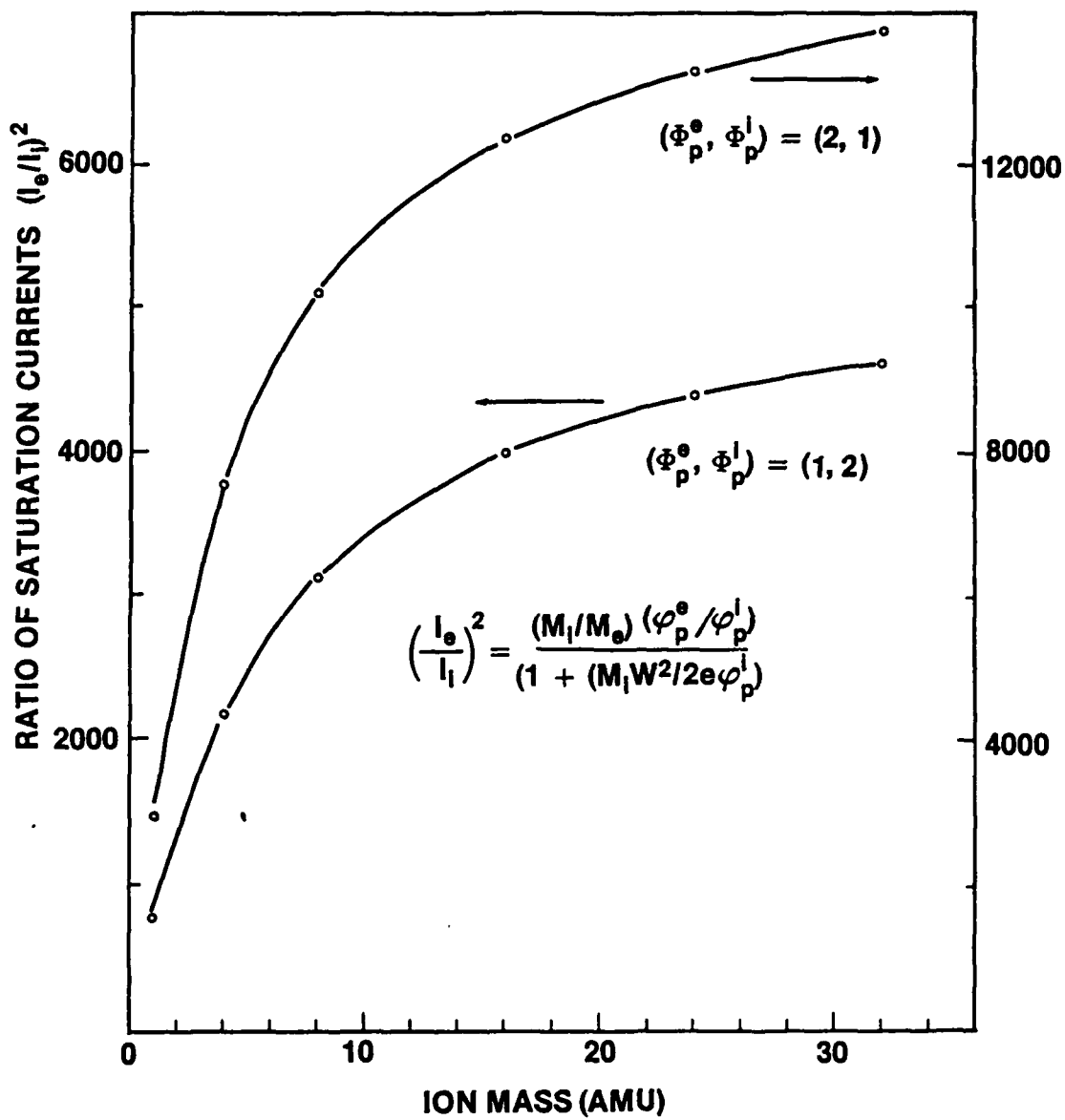


Fig. 3 — Dependence of the saturation current ratio $(I_e/I_i)^2$ on ion mass

DATA ANALYSIS AND RESULTS

Initial reduction routines for bulk processing and plotting of P⁴/S3-4 data begin with an orbit-by-orbit plot of relative electron density as measured by changes in ion- and electron-saturation currents. A representative sample of this data collected on orbit 2177 is shown in Figure 4 where the abscissa coordinates are universal time (UT), altitude (ALT in km), latitude (LAT), longitude (LONG), magnetic latitude (MLAT), and L-shell value (L). The probes' magnetic aspect angle is also plotted in the figure.

The left hand edge in Figure 4 corresponds to the satellite's ascending node (south-to-north) in the midnight hemisphere near the south magnetic pole (MLAT = -90°). With increasing time (UT) the satellite passes through the nighttime equator, the main trough, over the northern auroral oval and into the dayside ionosphere where vehicle solar cell voltage biases the entire vehicle such that both probes draw approximately equal ion saturation currents.

The simultaneous measurements of electron- and ion-saturation currents, $I_B(E)$ and $I_B(I)$ respectively, provide confidence that the observed irregularities involve plasma variations and not just secondary effects (e.g., aspect sensitivities and variations in spacecraft potential).

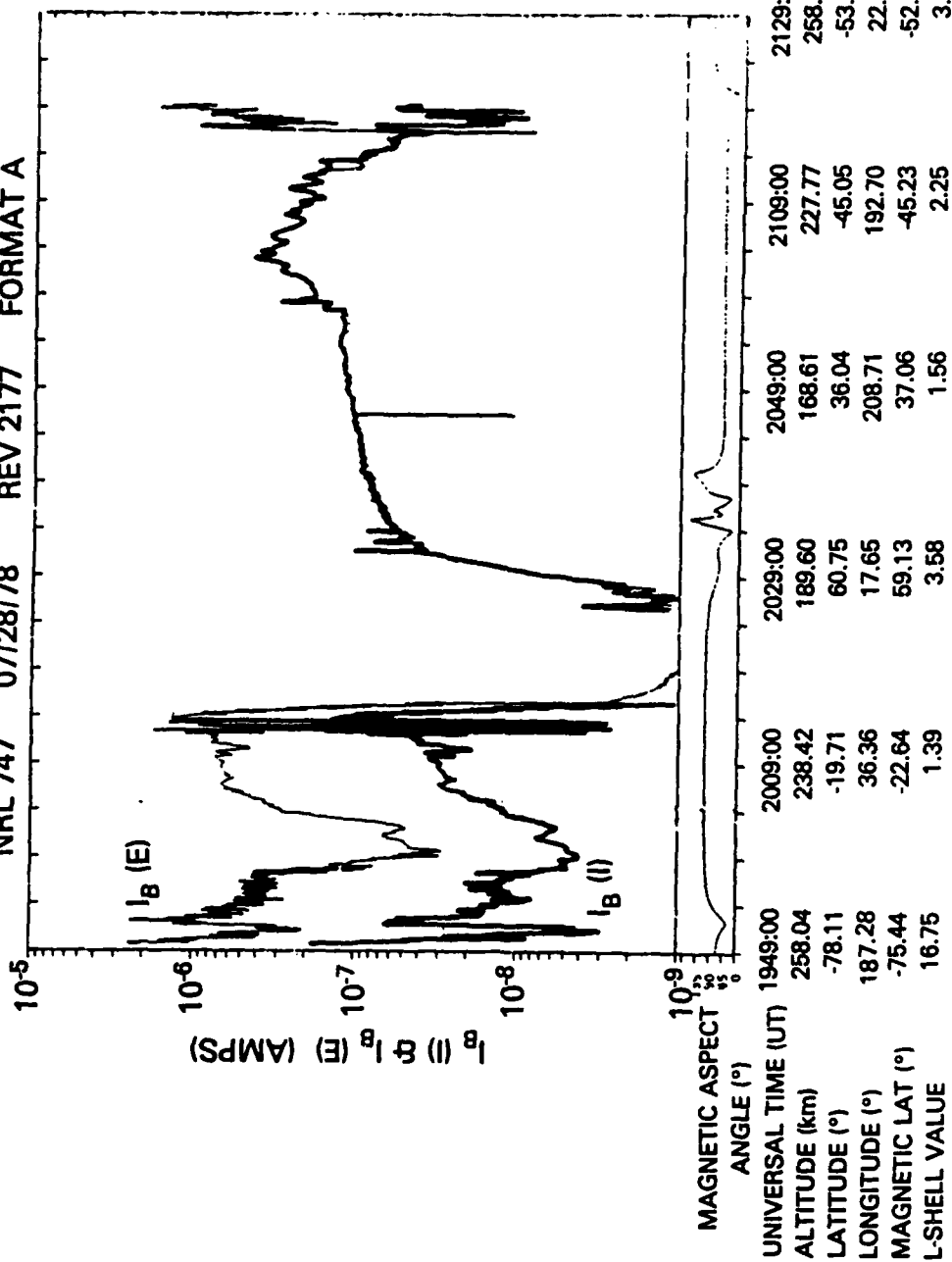


Fig. 4 — Relative electron density as measured on one complete orbit by the pulsed-plasma-probe experiment on the S3-4 satellite

Figure 4, characteristic of data accumulated to date, shows that the nighttime F-region is orders of magnitude more irregular than its dayside counterpart. The irregularities in the nighttime southern high-latitude region ($MLAT < -40^\circ$) is considered characteristic of that domain, with the most intense structures generally showing electron density variations less than an order of magnitude. There are other characteristic features in the data within $\pm 15^\circ$ of the nighttime equator, where observations of large scale plasma depletions (1 to 3 orders of magnitude) occur with a frequency typical of equatorial spread-F.

While data sets like that shown in Figure 4 provide a global map of large scale ionospheric features, primary investigative objectives are directed at the relationships between the large scale features and much smaller scale irregularities (tens of meters and less) believed to result from multistep plasma processes. To this end, the fundamental data sets $I_e(\text{sat})$ and $(I_e(\text{sat})/I_1(\text{sat}))^2$ are Fast Fourier analyzed to determine their density fluctuation power spectra, $P_N(k)$ and $P_M(k)$ respectively, where

$$\left| \frac{\delta I_e}{\bar{I}_e} \right|^2 \equiv \left| \frac{\delta N_e}{\bar{N}_e} \right|^2 + P_N(k) \quad (5)$$

and

$$\frac{\delta(I_e/I_1)^2}{(\bar{I}_e/\bar{I}_1)^2} \equiv \frac{\delta \bar{M}_1}{\bar{M}_1} + P_M(k) \quad (6)$$

The analytical relationship between $\delta N_e/\bar{N}_e$ and $\delta \bar{M}_1/\bar{M}_1$ can be simply established for a 2-component ion distribution of masses and densities (M_α, M_β) and (N_α, N_β) respectively. We do this by use of the definitions

$$\bar{M}_1 = \frac{M_\alpha N_\alpha + M_\beta N_\beta}{(N_\alpha + N_\beta)} \quad (6a)$$

$$N_e = N_\alpha + N_\beta \quad (6b)$$

$$N_\alpha = N_\alpha^0 + N_\alpha^1 \quad (6c)$$

$$N_\beta = N_\beta^0 + N_\beta^1 \quad (6d)$$

$$\delta N_e = \delta N_\alpha + \delta N_\beta = N_\alpha^1 + N_\beta^1 \quad (6e)$$

and a straightforward manipulation to derive

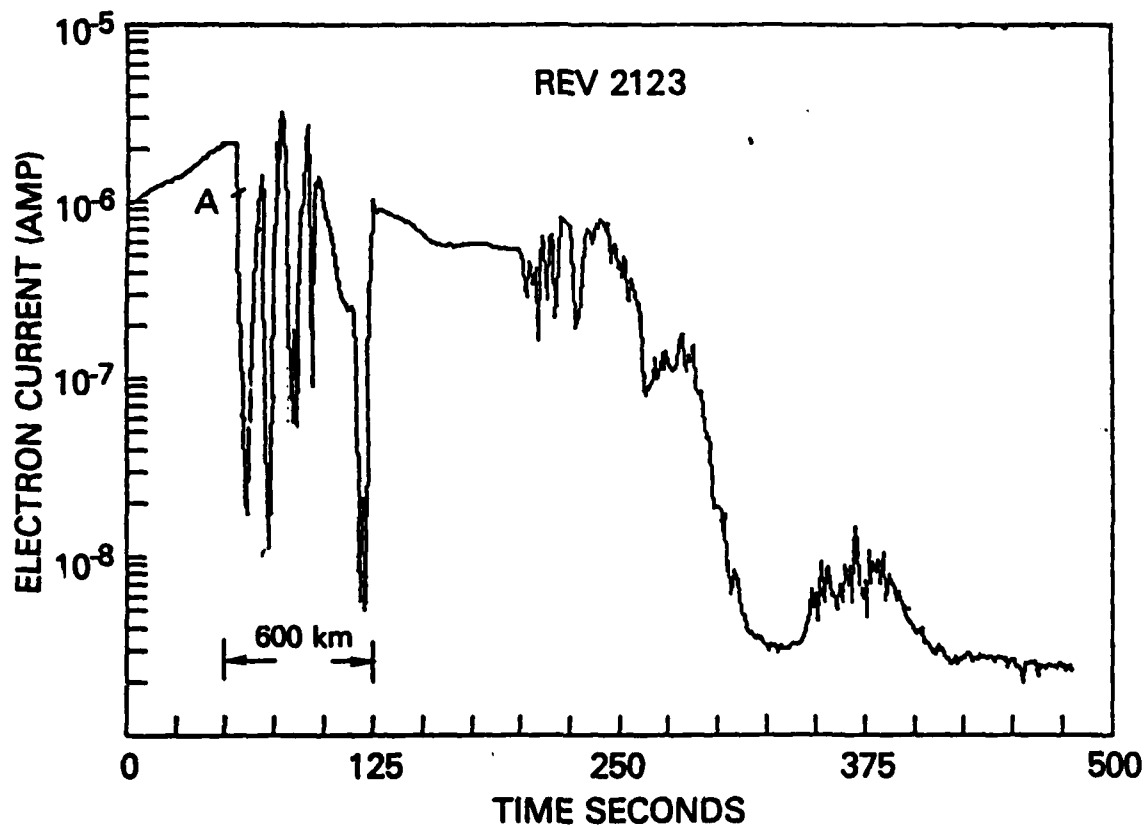
$$\frac{\delta \bar{M}_1}{\bar{M}_1} = \frac{\delta N_e}{\bar{N}_e} f(\alpha, \beta) \quad (7a)$$

where

$$f(\alpha, \beta) = \left\{ \frac{\left(\frac{M_\alpha}{M_\beta} \right) - 1}{\left(\frac{M_\alpha}{M_\beta} \right) \left(\frac{N_\alpha^0}{N_\beta^0} \right) + 1} \right\} \left\{ \frac{N_\alpha^1/N_\beta^1 - N_\alpha^0/N_\beta^0}{\left(N_\alpha^1/N_\beta^1 \right) + 1} \right\} \quad (7b)$$

It is appropriate to note that the experimental determination of mean-ion-mass fluctuations $\delta\bar{M}_1(+P_M)$, through variations in $[I_e(\text{sat})/I_1(\text{sat})]^2$, assumes the relative constancy of all potentials. (This includes the spacecraft potential as well as the potentials which each probe presents to the plasma.) The spacecraft potential can vary as a direct result of changes in local plasma density since the floating potential of a body is dependent upon the ratio of its radius to the Debye length. For large space vehicles however, floating potential variations caused by even substantial plasma density variations should be small (Szuszczewicz, 1972). Another possible source of potential variations involve charging of contamination layers on the vehicle and/or on the probes (Szuszczewicz and Holmes, 1975). From the S3-4 data examined to date, variations in $(I_e/I_1)^2$ associated with charging on contamination layers, appear to be a slowly varying function of time with no attendant effects on P_M . Therefore, we have concluded that the spectral dependence of P_M is indeed representative of variations in mean-ion-mass $\delta\bar{M}_1$.

To experimentally demonstrate $P_M(k)$ and the associated relationship with $P_N(k)$ consider the high-resolution measurements (rev #2123) of the relative electron density across the nighttime equator (Figure 5). The peak electron density is approximately $5 (10^5) \text{ cm}^{-3}$ at $I_B = 3 (10^{-6})$ amp. The large scale depletions are seen to extend to 2 orders of magnitude with widths ranging from 50 to 170 km over a 600 km orbital segment.



UT 10:50:22

ALT 241.1 km

LAT -18.71°S

LONG 175.9°E

10:58:42

219 km

11.9°N

170.3°E

Fig. 5 — An expanded view of relative electron density encountered during the nighttime equatorial crossing on S3-4 rev 2123. The relative electron density is presented by baseline electron saturation current.

In Figure 6 are presented the P_N and P_M results for a 1 second interval located by point A in the density profile of Figure 5. Fitting the results to a power law behavior we find

$$P_N = A_n f^{-2.9} \quad (8a)$$

and $P_M = A_m f^{-1.5} \quad (8b)$

By assuming that the time (frequency) domain spectral analysis in Figure 6 can be converted to wavelength through the vehicle velocity (7.53 km/sec), the experiment shows $f_N^{-2.9}$ ($\propto k^{-2.9}$) from $k \sim 2\pi/1 \text{ km}^{-1}$ to $k = 2\pi/20 \text{ meters}^{-1}$. This is the first such satellite determination to wavelengths as short as 20 meters, with the earlier work of McClure and Hanson (1973) having defined some of the spectral features of equatorial spread-F down to 70 meters. (Conversion to the component of k perpendicular to the geomagnetic field extends the low wavelength end of Figure 6 down to $k = 2\pi/6 \text{ meter}$, the approximate value for the O^+ Larmor radius.)

The spectral index for P_N is approximately 15% steeper than previously reported values for conditions of bottomside spread-F (Keskinen et al., 1981) but well within the distribution of S3-4 spectral indices currently being accumulated and analyzed (Singh, currently unpublished) for conditions identified with the intermediate wavelength domain ($k = 2\pi/1 \text{ km}^{-1}$ to $k = 2\pi/20 \text{ m}^{-1}$).

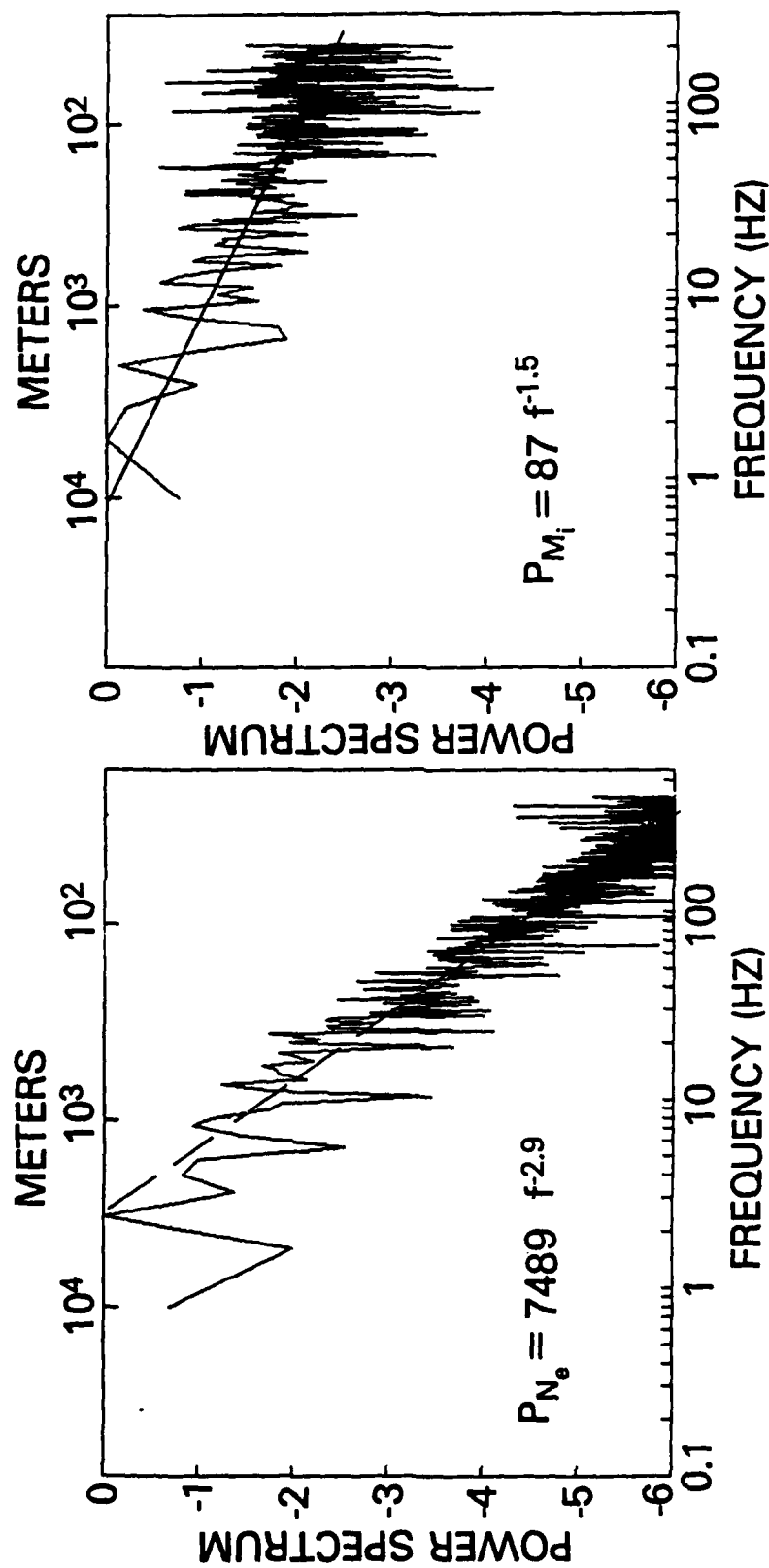


Fig. 6 — Sample illustration of simultaneously determined density fluctuation power spectrum P_N and mean ion mass fluctuation power spectrum P_M

The $P_M \propto f^{-1.5}$ observation is the first of its kind and unique to the NRL-747/S3-4 experiment. Currently there are no computational guidelines on the expected behavior, but there is sufficient evidence in laboratory plasma studies to warrant such systematic considerations of ions and their role in the hierarchy of possible mechanisms covering the spectrum of observed ionospheric irregularities. The importance of ions is clear...even from the simple considerations of the Rayleigh-Taylor instability in which a difference in charged-particle drift velocities produces an electric field across a horizontal perturbation. These drift velocities are mass dependent ($\bar{V}_i \propto M_i(\bar{g} \times \bar{B})/B^2$) and vary directly as the mass of the i^{th} species. Similar mass discriminatory effects play an important role in ambipolar diffusion processes across gradients in plasma density. The process operates more rapidly on lighter ions and can result in "patches" of varying ion mass, with local variations in conductivity and electric fields, and ultimately an ion dependent interaction in the process of energy dissipation in the large-to-small scale irregularity distribution. The P_M measurement has been designed to test for just that type of interactive mode.

$\delta \bar{M}_1 / \bar{M}_1$ is a fairly complicated function of M_α / M_β , N_α^0 / N_β^0 , N_α^1 / N_β^1 and $\delta N_e / \bar{N}_e$ itself (See Eq. 7b); and at this point we can only speculate on the many manifestations that P_N and P_M might take for the varied ionospheric conditions encountered in the S3-4 mission. For example, it has been suggested (J.R. Goldman, private communication) that differences in gradient scale lengths for N_e and $M_{\alpha,\beta}$'s would result in a more rapid fall off with increasing k for the quantity with an initially larger gradient scale length. This difference should be a direct observable through the P_N and P_M determination. Furthermore, there is the possibility that the simultaneous measurement of $P_M(k)$ could help differentiate between a k^{-2} spectrum due to sharp edges and a k^{-2} spectrum due to gradient-drift or say drift-dissipative waves.

Currently, we have not analyzed sufficient data to exact any of the above analyses. We are at the beginning of a synoptic study designed to systematically unfold the interdependence of P_N and P_M , and the contributing roles of ion mass distributions through M_α / M_β and N_α^0 / N_β^0 . However, the results in Figure 6 as well as in Figure 7 can be used to reflect some of our observations:

(i) The absolute power in P_N is generally much greater than that in P_M . In Figure 6, for example, power law fits yield $A_n / A_m \sim 86$, reflecting a situation in which the absolute density fluctuations $\delta N_e / \bar{N}_e$ are two orders of

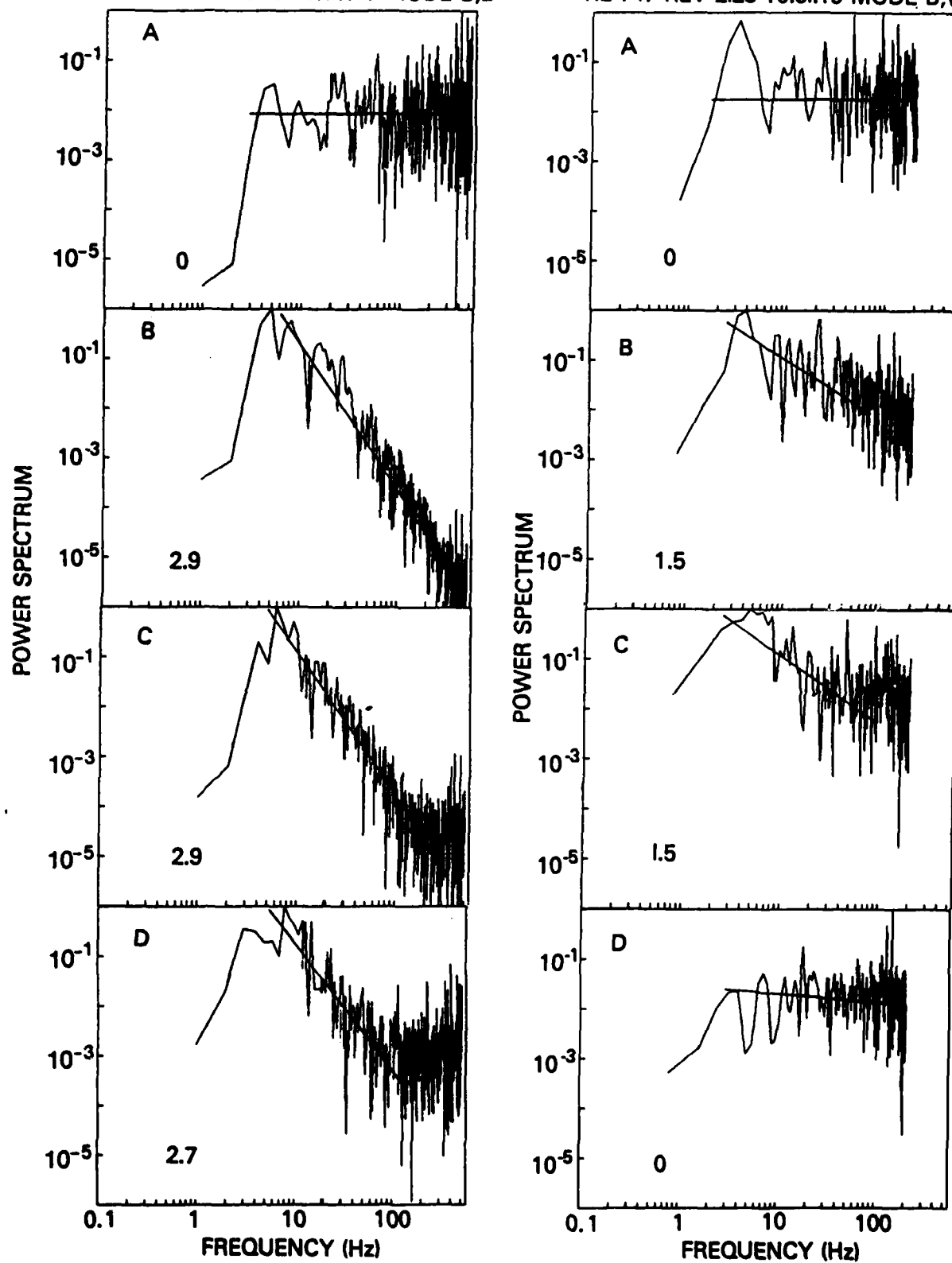


Fig. 7 — Four contiguous FFT's of electron density fluctuations (left side A through D) and simultaneously determined fluctuations in mean ion mass (right side A through D)

magnitude more intense than counterparts in $\delta\bar{M}_1/M_1$.

(ii) More often than not the k-dependence of P_N is maintained to shorter wavelength (higher frequencies) than $P_M(k)$.

(iii) The relationship between the spectral indices of P_N and P_M is highly variable. Figure 7 is an illustration of a random selection of 1.2-second interval spectra near the domain sampled in Figure 6. Panel A represents the power spectrum of the quiescent region before the depletion, while panels B through D represent contiguous power spectra within the depletion. In the quiescent region (Panel A), both density and mean ion mass fluctuations show noise spectra, while inside the depletion well-defined k-dependencies in P_N and (less frequent) k-dependent spectra in P_M are observed. While small in number, this sample of data is rather representative of results accumulated to date. More frequently than not P_M is equal to or softer than P_N (e.g., panels B, C and D). In addition, there are observations of well-defined k-spectra in P_N with none in P_M (i.e., only noise, as in panel D). Panel D is interpreted as an unstable plasma environment with a single component ion population. This is in agreement with the predictions of Eq. (7b) with $M_\alpha = M_\beta$.

Results like those outlined above are continuing with a view to a synoptic definition of the P_M , P_N interdependence and the associated roles of \bar{M}_1 , gradient scale lengths and geoplasma conditions (N_e , T_e and MLAT).

COMMENTS AND CONCLUSIONS

In order to develop a more comprehensive experimental profile on ionospheric irregularities, the pulsed plasma probe technique has been expanded to include the measurement of mean ion mass and associated mass variations, $\delta M_i / M_i$, on a spatial scale limited only by geometry and telemetry. Conducted simultaneously with the standard determinations of absolute density N_e , temperature T_e , and density fluctuation power spectra $\delta N_e / \bar{N}_e \rightarrow P_N(k)$, the expanded capability has opened up investigations which explore the coupling of electron and ion plasma wave energies which may influence the way in which large scale plasma perturbations cascade to much smaller dimensions.

Although the relationship between $\delta M_i / \bar{M}_i$ and $\delta N_e / \bar{N}_e$ is a complicated function of ratios in the ion populations, i.e., M_α / M_β , N_α^0 / N_β^0 , N_α^1 / N_β^1 , it may be systematically related to absolute densities, gradient scale lengths and time in cascading instability processes.

The new technique has been successfully flown on an F-region, polar orbiting satellite with some of the early results including:

(1) Extension of δN_e measurement capability down to dimensions of the order 5-20 meters, with associated power spectra of spectral index in the range 1.6 to 2.9. While short of the 1-3 meter limit desirable for comparison with Jicamarca or Altair radar coherent scatter results, the S3-4

experiment goes beyond the 70 meter limit of earlier satellite measurements and lends itself to additional arguments which support the association of the Rayleigh-Taylor instability occurrence of equatorial spread-F.

(2) Measurements of $\delta \bar{M}_1$ with resolution that allows detection of macroscale features (e.g., transitions from O^+ dominant to NO^+ dominant environment) and microscale spectral analysis down to dimensions comparable to the δN_e capability. As expected, power law fits ($P(k) = Af^{-X}$) to P_N and P_M have revealed considerable variations with X_M generally (but not always) smaller than X_N . Similarly, the absolute power A_M in ion mass fluctuations have been found to be considerably less (@ 2-100) than the power in P_N . A systematic study of the detailed relationships and dependence on zero-order plasma conditions is currently underway.

ACKNOWLEDGMENT

The authors wish to thank the Air Force Space Test Program, the Naval Space Systems Activity and the Office of Naval Research for support throughout this program. We are also indebted to M. G. Swinney and L. S. Kegley for their diligent efforts in all phases of fabrication, testing and integration. This work was supported within the Ionospheric and Stratospheric Task Area (09490) and conducted within the Ionospheric Diagnostics Section of the Space Science Division.

REFERENCES

- Brinton, H.C., Mayr, H.G. and Newton, G.P., "Ion composition in the nighttime equatorial F-region: Implications for chemistry and dynamics (abstract)", EOS Trans. AGU 56, 1038 (1975).
- Chen, F.F., "Electrical probes", in Plasma Diagnostic Techniques, ed. by R.H. Huddestone and S.L. Leonard (Academic, N.Y. 1965) p. 113.
- Dyson, D.L., McClure, T.P. and Hanson, W.B., "In situ measurements of spectral characteristics of F-region ionospheric irregularities", J. Geophys. Res. 79, 1497 (1974).
- Hoegy, W.R. and Wharton, L.J., "Current to a moving cylindrical electrostatic probe", J. Appl. Phys. 44, 5365 (1973).
- Holmes, J.C. and Szuszczewicz, E.P., "The versatile plasma probe", Rev. Sci. Instr. 46, 592 (1975).
- Huba, J.C., Chaturvedi, P.K., Ossakow, S.L. and Towle, D.M., "High frequency drift waves with wavelengths below the ion gyro radius in equatorial spread-F", Geophys. Res. Lett. 5, 695 (1978).
- Kelley, M.C., Pfaff, R., Baker, K.D., Ulwich, J.C., Livingston, R., Rino, C. and Tsunoda, R., "Simultaneous rocket probe and radar measurements of equatorial spread-F-transitional and short wavelength results", J. Geophys. Res. (1981, in press).
- Keskinen, M.J., Ossakow, S.L. and Chaturvedi, P.K., "Preliminary report on numerical simulations of intermediate wavelength collisional Rayleigh-Taylor instability in equatorial spread-F", J. Geophys. Res. 85, 1775 (1980).

- Keskinen, M.J., Szuszczewicz, E.P., Ossakow, S.L. and Holmes, J.C., "Nonlinear theory and experimental observations of the local collisional Rayleigh-Taylor instability in a descending equatorial spread-F ionosphere", J. Geophys. Res. 86, 5785 (1981).
- McClure, J.P. and Hanson, W.B., "A catalog of ionospheric F-region irregularity behaviour based on OGO-6 retarding potential analyzer update", J. Geophys. Res. 78, 7431 (1973).
- McClure, J.P., Hanson, W.B. and Hoffman, J.H., "Plasma bubbles and irregularities in the equatorial ionosphere", J. Geophys. Res. 82, 2650 (1977).
- Narcisi, R.S. and Szuszczewicz, E.P., "Direct measurements of electron density, temperature and ion composition in an equatorial spread-F ionosphere", J. Atm. Terr. Phys. 43, 463 (1981).
- Ossakow, S.L., "Research at NRL on theoretical and numerical simulation studies of ionospheric irregularities", NRL Memorandum Report #2907, (Oct. 1974).
- Ossakow, S.L., Zalesak, S.T., McDonald, B.E. and Chaturvedi, P.K., "Nonlinear equatorial spread-F: Dependence on altitude of the F-peak and bottomside background electron density gradient scale length", J. Geophys. Res. 84, 17 (1979).
- Rodriguez, P., Singh, M., Szuszczewicz, E.P., Walker, D.N., and Holmes, J.C., "The STP/S3-4 satellite experiment: High latitude large scale density irregularities", Proceedings of the Ionospheric Effects Symposium, (ed. by J.M. Goodman, Govt. Printing Office), (1981, in press).

- Singh, M., Szuszczewicz, E.P. and Holmes, J.C., "The STP/S3-4 satellite experiment: Equatorial F-region irregularities", Proceedings of the Ionospheric Effects Symposium, (ed. by J.M. Goodman, Govt. Printing Office), (1981, in press).
- Szuszczewicz, E.P., "Area influences and floating potentials in Langmuir probe measurements", J. Appl. Phys., 43, 874 (1972).
- Szuszczewicz, E.P. and Holmes, J.C., "Surface contamination of active electrodes in plasmas: Distortion of conventional Langmuir probe measurements", J. Appl. Phys. 46, 5137 (1975).
- Szuszczewicz, E.P. and Holmes, J.C., "Observations of electron temperature gradients in mid-latitude E_s layers", J. Geophys. Res. 82, 5073 (1977).
- Szuszczewicz, E.P., "Ionospheric holes and equatorial spread-F: Chemistry and transport", J. Geophys. Res. 83, 2665 (1978).
- Szuszczewicz, E.P., Tsunoda, R.T., Narcisi, R. and Holmes, J.C., "Coincident radar and rocket observations of equatorial spread-F", Geophys. Res. Lett. 7, 537 (1980).
- Szuszczewicz, E.P., Holmes, J.C. and Singh, M., "Satellite and rocket observations of equatorial spread-F irregularities: A Two-dimensional model", J. Atm. Terr. Phys., (1981, in press).